Department of Industrial Engineering and Management Sciences

Northwestern University, Evanston, Illinois, 60208-3119, U.S.A.

Working Paper No. 12-02

Time-Optimal Trajectories with Bounded Curvature in Anisotropic Medium

Irina S. Dolinskaya

Department of Industrial Engineering and Management Sciences, Northwestern University

e-mail: dolira@northwestern.edu

Alvaro Maggiar

Department of Industrial Engineering and Management Sciences, Northwestern University

e-mail: alvaromaggiar2014@u.northwestern.edu

This work was supported in part by the Office of Naval Research through the Multidisciplinary University Research Initiative (MURI) Optimum Vessel Performance in Evolving Nonlinear Wave Fields grant (N00014-05-1-0537) and through the Autonomous Vehicle Dynamic Navigation System grant (N00014-11-1-0516).

June 7, 2012

Time-Optimal Trajectories with Bounded Curvature in Anisotropic Medium

Irina S. Dolinskaya * Alvaro Maggiar †

Abstract

This paper characterizes time-optimal trajectories in anisotropic (direction-dependent) environments where path curvatures are bounded by the minimum turning radius of a mobile agent. Such problems are often faced in the navigation of aerial, ground and naval vehicles when a mobile agent cannot instantaneously change its heading angle. The presented work is a generalization of the Dubins car problem, which considers fastest paths with bounded curvature while assuming constant speed and minimum turning radius. We relax this assumption and discuss fastest-path finding problems for the generalized direction-dependent speed and minimum turning radius functions, to account for the effects of waves, winds and slope of the terrain on the agent's motions. We establish that there exists an optimal path such that it is a portion of a path of the type $\mathcal{CSCSC}$ where $\mathcal{C}$ denotes a sharpest turn curve and $\mathcal{S}$ a straight line segment. Further analysis of a special case (wherein the speed polar plot is convex) delivers a more detailed characterization of an optimal path and presents an algorithm that implements our results.

Keywords: Nonholonomic motion planning, Dubins vehicle, optimal path finding, anisotropic environment, optimal control.

1 Introduction

This paper addresses optimal path finding problems with bounded curvature in an *anisotropic* (i.e., direction-dependent) environment. Such problems are encountered in sailing, robotics and aerial vehicle navigation, where the agent's motion is affected by the direction of waves, winds or slope of the terrain, and the control system of an agent constrains the set of permissible paths. Our objective is to find a path that minimizes the travel time and ends at a pre-specified destination point and heading angle, given that it starts at an initial point with a known heading angle and has its curvature bounded by a specified minimum turning radius function. The effect of an anisotropic environment on the agent's motion results in a direction-dependent speed function. Furthermore, the direction-dependence of the speed extends to the minimum turning radius function. The curvature constraint of a feasible path is often a function of speed, such as in the case of a surface vessel where a higher traveling speed causes greater forces on its rudder and enables sharper turns. Therefore, both the agent's speed and minimum turning radius are described by the direction-dependent functions in an anisotropic medium.

Current research regarding the optimal short-range routing of a vessel in a stationary random seaway characterized by a *sea state* (parameter describing wavefield distribution), Dolinskaya et al. (2009), motivated our work. In such a setting, the added resistance of the surface vehicle in irregular waves is integrated with the operability constraints (such as, root-mean-squared roll and probability of wet deck) to deliver the expected maximum attainable vessel speed, as a function of its heading, relative to the dominant wave direction. The resulting speed function (see Figure 1) is used to evaluate the fastest path. It is important to note that the speed functions in this setting have a more complex structure than in the preceding work in the literature studying an agent's motion in the presence of constant wind or current field. The direction-dependence of the speed function in Dolinskaya et al. (2009) does not only capture the direct effect surrounding waves have on the vessel speed, but also reflects the vessel's voluntary speed

*corresponding author; Department of Industrial Engineering and Management Sciences, Northwestern University, 2145 Sheridan Road, Evanston, IL, 60208 USA e-mail: dolira@northwestern.edu.

†Department of Industrial Engineering and Management Sciences, Northwestern University, Evanston, IL, 60208 USA.

reduction necessary to satisfy the operability constraints. Furthermore, the short range of the trips and stationary distribution of the wavefield considered in this application support our assumption of time and space homogeneous environments (which we relax in the future work). In this paper we extend the research of Dolinskaya et al. (2009) and Dolinskaya & Smith (2012) to incorporate the minimum turning radius constraint restricting vessel maneuverability.

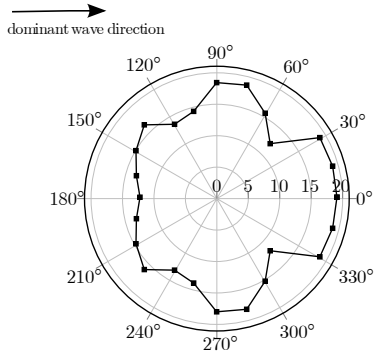

Figure 1: An example of speed polar plot for the S175 containership in Sea State 7 irregular wavefield (adapted from Dolinskaya et al. (2009))

We incorporate two characteristics into our optimal-path finding problem: (1) the direction-dependent nature of the environment and (2) the curvature constraint of the sharpest feasible turns that a mobile agent can perform. Each of these additional characteristics considerably complicates the original analysis of the agent's optimal path. Incorporating both characteristics simultaneously also further increases complexity of the optimal vehicle navigation problem.

(1) The difficulty of optimal-path finding in an anisotropic medium (even without the sharpest turn constraint) comes from the fact that the cost associated with traversing a straight line segment from a to b does not necessarily equal the cost of traveling the reversed straight line path from b to a. Thus, the cost function for this simpler special case problem that permits instantaneous heading change is not a metric. Furthermore, the anisotropic cost, in general, violates the triangle inequality, making it suboptimal to follow a straight line path even if it is a control feasible action.

(2) In an anisotropic environment where the minimum turning radius is a function of the agent's heading, the curvature of the sharpest turn changes as the vehicle alters its heading angle in the process of turning. This non-constant turning radius results in complex sharpest turn curves, as opposed to circle arcs which are an essential part of an optimal path for the isotropic problems. Dynamic turning radii result in a complex set of feasible curves that an optimal-path may contain, which significantly complicates the problem of finding an optimal path with minimum curvature in the anisotropic case.

The presented work relaxes the assumption of the Dubins car problem (Dubins, 1957) of constant speed and curvature constraint, and extends the results to the generalized fastest-path finding problems with arbitrary direction-dependent speed and minimum turning radius functions. We establish that there exists an optimal path such that it is a portion of a path of the type $\mathcal{CSCSC}$ where $\mathcal{C}$ denotes a sharpest turn curve and $\mathcal{S}$ a straight line segment. Further analysis of a special case (wherein the speed polar plot is convex) delivers a more detailed characterization of an optimal path (similar in structure to the solution of a Dubins car problem) and presents an algorithm that implements our results.

It is important to note that the assumption of time and space homogenous environment of this paper are relaxed in our forthcoming work, which generalizes the problem. The results presented in this paper are integrated into the more general model and are essential to computationally efficient algorithms we develop for time and space dependent problems.

1.1 Related Work

L. E. Dubins introduced the optimal path with bounded curvature problem, also known as the Dubins car problem, in 1957 (Dubins, 1957). Dubins' critical assumption was that vehicle speed and the minimum turning radius are constant and do not depend on the direction. His intricate set of geometric statements and propositions show that "an R-geodesic is necessarily a continuous differentiable curve which consists

of not more than three pieces, each of which is either a straight line segment or an arc of a circle of radius R." Two independent research teams, Boissonnat et al. (1994) and Sussmann & Tang (1991), simplify the proof by employing techniques of modern control theory and the minimum principle of Pontryagin (Pontryagin et al., 1962). To further the study of this problem, Bui et al. (1994) and Souères & Laumond (1996) computed a synthesis of the shortest paths by partitioning the configuration space $\mathbb{R}^2 \times S^1$ into cells reachable by the same configuration type of the shortest path.

The optimal control theory based approach to Dubins car problem generated great interest within the field of robotics, and numerous variations and extensions of the problem are discussed in the literature. Reeds & Shepp (1990) studied optimal paths with bounded curvature for a car that moves forward and backwards, resulting in paths with cusps. Boissonnat et al. (1994) proposed a dynamic extension of the Dubins car problem by constraining the angular acceleration of the agent instead of its angular velocity. Bakolas & Tsiotras (2009) extended the analysis to an asymmetric problem where radii for clockwise and counterclockwise sharpest turns are different. Some researchers considered problems with more complex mobile robot configuration such as trailer-truck systems navigation (Souères & Boissonnat, 1998) and the shortest distance for polygonal robot to an obstacle (Vendittelli et al., 1999; Giordano et al., 2006; Giordano & Vendittelli, 2009). Chitsaz & LaValle (2007), on the other hand, extended Dubins car to consider altitude, which led to time-optimal trajectory for aircraft problems. Other related problems discuss optimal path planning for differential-drive robots (Balkcom & Mason, 2002; Chitsaz et al., 2009; Bhattacharya et al., 2007), omni-directional vehicles (Balkcom et al., 2006), and bidirectional steering robots (Wang et al., 2009). Despite the wide variety of the aforementioned extensions, the assumption of constant speed and minimum turning radius (or angular acceleration in the case of (Boissonnat et al., 1994)) restricted the analysis to isotropic cases.

Some work addresses the direction-dependent problems by considering specific applications. Unmanned aerial vehicle (UAV) routing is the predominant area of such applications, where researchers analyze the effect of the directional winds on the UAV optimal paths. In such cases, the realized velocity of the aircraft is equal to the vector sum of the nominal vehicle velocity in the wind-free environment and the wind velocity. In the majority of published work (Osborne & Rysdyk, 2005; McGee et al., 2006; Techy & Woolsey, 2009; Bakolas & Tsiotras, 2010) in this area, the vehicle nominal speed and the wind speed are assumed to be constant, which imposes a specific structure on the actual direction-dependent speed function and the minimum turning radius of an agent. In fact, Rysdyk (2007) demonstrated that a vehicle making the sharpest feasible turn in the presence of a constant wind field follows a trochoidal path. We make no such restrictions in our forthcoming analysis to address a more general set of problems.

McNeely et al. (2007) considered the problem of constructing a minimum-time trajectory for UAVs in the presence of a time-dependent wind vector field. Analogous to the work discussed above, the realized velocity of a vehicle is computed by adding the wind vector field to a constant-magnitude velocity of the agent. To solve their problem, McNeely and colleagues transformed space by the wind vector, implemented Dubins car solution in the new space, and iteratively applied Newton's method to converge to the correct destination (boundary condition). The authors proved the existence and uniqueness of an optimal solution, along with the convergence of the algorithm.

1.2 Overview of the Results

This paper furthers the existing research by explicitly characterizing the structure of an optimal path with bounded curvature in an anisotropic environment. Without making assumptions regarding the structure of either the direction dependent speed function nor the minimum turning radius function, we establish the system's controllability, demonstrate the existence of an optimal path, and invoke optimal control theory techniques to derive a necessary condition for optimality. The subsequent analysis further investigates the structure of an optimal path, resulting in a systematic characterization of such a path and an algorithm that implements the results in the case of a convex speed polar plot.

We establish that there exists an optimal path such that it is a portion of a path consisting of three sharpest turn curves, denoted by $\mathcal{C}$, alternating with two straight line segments, denoted by $\mathcal{S}$. (i.e., of the form $\mathcal{CSCSC}$, see Theorem 25). In the case where the speed polar plot is convex, we show that the structure of an optimal path is similar to the solution of the Dubins car problem and consists of either three sharpest turn arcs with an alternating direction (i.e., $\mathcal{CCC}$), or a sharpest turn curve followed by a straight line segment and concluded by a second sharpest turn arc (i.e., $\mathcal{CSC}$). It is important to note that while the characterization of optimal paths for the Dubins car problem and our generalized problem

with convex speed polar plot are similar, the sharpest turn curves in our results have a general, and often complex, structure (not necessarily circle arcs as for Dubins car problem).

The rest of the paper is organized as follows. Section 1.3 presents the precise problem statement, including a list of technical assumptions necessary to ensure the rigorous analysis throughout the paper. Section 2 demonstrates the problem's controllability (by employing the controllability of the Dubins car problem), proves the existence of an optimal path (via Filippov's Theorem), and derives a necessary condition for optimality (using Pontryagin's Principle). In Section 3, we employ an optimality condition and further analyze the problem structure to deliver an optimal path. First, we examine the problem in the case of a general direction-dependent speed function, and then in the case when the speed polar plot is convex. This section also presents Algorithm 1, which implements our results for the convex case and delivers an explicit path finding procedure. Section 4 illustrates an application of our key results to the optimal short-range routing of a vessel in a stationary random seaway problem that motivated our work. Finally, Section 5 concludes the paper with a summary of the results and discusses future work. The Appendix contains the proofs omitted in our main discussion, as well as supporting calculations for the numerical results of Section 4.

1.3 Problem Statement

Consider a point vehicle, and let $(x, y, \theta) \in \mathcal{M} = \mathbb{R}^2 \times S^1$ denote the vehicle *configuration*, where (x, y) are the coordinates of the vehicle *position* and θ is the *orientation* (or *heading angle*) of the vehicle with respect to the x axis. For a given starting configuration (x_s, y_s, θ_s) and a given target configuration (x_t, y_t, θ_t), the problem objective is to find an *optimal path* (or a *fastest path*) from (x_s, y_s, θ_s) to (x_t, y_t, θ_t). We define the optimal path as a feasible path that minimizes vehicle travel time. Here, the curvature of a *feasible path* is restricted by a minimum turning radius function $R(\theta) : S^1 \to \mathbb{R}^+$ dependent on the vehicle heading angle. The anisotropic speed function $V(\theta) : S^1 \to \mathbb{R}^+$ denotes the maximum attainable speed that the vehicle can achieve at each orientation. Without loss of generality, we assume the vehicle starts its travel from (x_s, y_s, θ_s) at time $t_0 = 0$.

For completeness, we state the following assumptions to be used in the analysis.

Assumption 1. *The mobile agent's speed is always equal to its maximum attainable speed $V(\theta)$.*

Without loss of optimality, the speed of a mobile agent is assumed to be a fixed parameter specified for each instance of the problem. Nevertheless, it is worth noting that for some applications this assumption is too restrictive. Intuitively, in a time-homogeneous medium it never appears to be advantageous to voluntarily decrease the speed. However, it is beneficial to reduce the speed if a lower speed may permit sharper turns and result in shorter paths. In such a scenario, the minimum turning radius function R explicitly depends on the vehicle speed, in addition to the heading angle. To address such problems, one would have to add a speed control variable to the decision space of the system, significantly increasing the complexity of a model. The relaxation of Assumption 1 is an interesting extension to be considered in our future work.

Assumption 2. *The minimum turning radius function $R(\theta)$ and the speed function $V(\theta)$ can only take on positive values, i.e., $R(\theta) > 0, \forall \theta \in S^1$ and $V(\theta) > 0, \forall \theta \in S^1$.*

Assumption 3. *The minimum turning radius $R(\theta)$ and the speed function $V(\theta)$ are $\mathcal{C}^\infty$ functions in θ.*

From Assumption 3 it follows that the functions $R(\theta)$ and $V(\theta)$ are bounded, that is, $\exists R_{\max}$ and $\exists V_{\max}$, such that $R(\theta) \leq R_{\max}$ and $V(\theta) \leq V_{\max}$, $\forall \theta \in S^1$.

2 Optimal Control Modeling and Analysis of the Problem

In this section, we demonstrate the problem's controllability, prove the existence of an optimal path, and apply optimal control theory techniques to derive the system's necessary condition for optimality.

2.1 Control Model

Define the state of the system to be $(x(t), y(t), \theta(t)) \in \mathcal{M}$, which is the vehicle configuration at time $t \in [0, T]$ (see Figure 2). We set the system steering controller $u(t) : [0, T] \to U$ to represent the rate

of change of the vehicle heading at time t, where U is the *control region* (i.e., the set of values that an admissible controller can take).

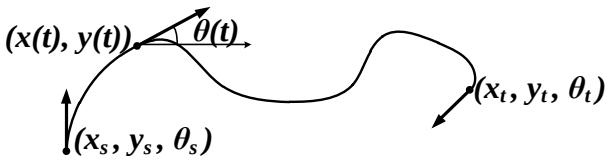

Figure 2: The state of the system is $(x(t), y(t), \theta(t))$, where $(x(t), y(t))$ is the position of a vehicle in $\mathbb{R}^2$ and $\theta(t)$ is its heading angle at time t.

The differential system describing the dynamics of our system is

$$\dot{x} = f_1(x, y, \theta, u) = V(\theta)\cos(\theta), \tag{1}$$
$$\dot{y} = f_2(x, y, \theta, u) = V(\theta)\sin(\theta), \tag{2}$$
$$\dot{\theta} = f_3(x, y, \theta, u) = \frac{V(\theta)}{R(\theta)}u, \tag{3}$$
$$\dot{x}_0 = f_0(x, y, \theta, u) = \frac{\sqrt{\dot{x}^2 + \dot{y}^2}}{V(\theta)} = 1, \tag{4}$$

with the boundary conditions:

$$(x(0), y(0), \theta(0)) = (x_s, y_s, \theta_s), \tag{5}$$
$$(x(T), y(T), \theta(T)) = (x_t, y_t, \theta_t), \tag{6}$$
$$x_0(0) = 0. \tag{7}$$

Quantity $x_0(t)$ denotes the travel cost accumulated by time t. Then, our objective is to minimize the total travel time denoted by J_u, which we define as

$$J_u = x_0(T) = \int_0^T f_0(x(t), y(t), \theta(t), u(t))dt = T. \tag{8}$$

Note that while the minimum turning radius $R(\theta)$ depends on the heading along the path, to facilitate our analysis we set the control region $U = [-1, 1]$, independent of the system state. Then we scale the path curvature by the residual of a minimum turning radius, $1/R(\theta)$, as can be seen in (3). (Assumption 2 guarantees that we never divide by zero.)

2.2 System Controllability

The first step to finding an optimal path is to prove that the problem is *controllable*, i.e., that there exists a feasible path for all possible starting and target states of the system. The Dubins car problem which finds the fastest path with bounded curvature with constant speed is controllable for a constant minimum turning radius $R_D(\theta) = r$ and a constant speed $V_D(\theta) = v$ for all $\theta \in S^1$ (see (Sussmann & Tang, 1991)). From Assumption 3 it follows that the minimum turning radius function is bounded above (since S^1 is a compact set) and there exists a minimum turning radius value large enough to be feasible for all headings, i.e., let $R_{\max} = \max_{\theta \in S^1} R(\theta)$. Similarly, Assumption 2 ($V(\theta) > 0, \forall \theta \in S^1$) ensures that there exists a minimum speed small enough to be feasible for all headings, that is, $V_{\min} = \min_{\theta \in S^1} V(\theta) > 0$.

Thus, the problem of fastest-path finding with bounded curvature restricted by the minimum turning radius $R_{\max}$ with the speed value $V_{\min}$ for all headings is equivalent to the Dubins car problem, which has been shown to be controllable (see (Sussmann & Tang, 1991)). Thus, to find a feasible path for a given instance of our problem we can solve a Dubins car problem with $R_D = R_{\max}$ and $V_D = V_{\min}$. Any feasible trajectory for this instance of Dubins car problem is also feasible for our initial problem, and

the controllability of the Dubins car problem yields controllability to our problem. Consequently, we can always find a feasible path from a given starting vehicle configuration (x_s, y_s, θ_s) to a given destination configuration (x_t, y_t, θ_t), thus proving that our problem is controllable.

2.3 Existence of an Optimal Path

To prove the existence of an optimal path, we apply Filippov's general theorem (Filippov, 1962) for minimum-time problems as presented by Souères & Boissonnat (1998, section 3.2). Observe that $\mathcal{M}$ is an open subset of $\mathbb{R}^3$, U is a subset of $\mathbb{R}$, and $f := (f_1, f_2, f_3)'$ is a linear function of the control parameter u, (1)-(3). For an optimal path to exist between any two points (x_s, y_s, θ_s) and (x_t, y_t, θ_t) in $\mathcal{M}$, the following four hypotheses must be satisfied:

1. f is a continuous function of $t, u, (x, y, \theta)$ and a continuously differentiable function of (x, y, θ).
2. The control set U is a compact subset of $\mathbb{R}$. Furthermore, when u varies in U, the image set described by $f(x(t), y(t), \theta(t), u(t))$ is convex for all $t, (x, y, \theta) \in [0, T] \times \mathcal{M}$.
3. There exists a constant C such that for all $(t, x, y, \theta) \in [0, T] \times \mathcal{M}$: $\langle (x, y, \theta), f(x, y, \theta, u) \rangle \leq C(1 + ||(x, y, \theta)||^2)$.
4. There exists an admissible trajectory from (x_s, y_s, θ_s) to (x_t, y_t, θ_t).

From Assumption 3 it follows that f is a continuous function of t and u and a continuously differentiable function of (x, y, θ), so the first hypothesis is satisfied.

Furthermore, the control set $U = [-1, 1]$ is a compact convex subset of $\mathbb{R}$, and when u varies in U for any $(x, y, \theta) \in \mathcal{M}$, the image set described by $f(x, y, \theta, u)$ is the image of a convex set via a linear function and is thus also convex.

Following a discussion similar to (Bakolas & Tsiotras, 2010), we show that there exists a constant C such that for all $(t, x, y, \theta) \in [0, T] \times \mathcal{M}$, $|\langle (x, y, \theta), f(x, y, \theta, u) \rangle| \leq C(1 + \|(x, y, \theta)\|^2)$. We apply the Cauchy-Schwartz inequality and other norm space and trigonometric properties in the following derivation:

$$\begin{aligned} |\langle (x, y, \theta), f(x, y, \theta, u) \rangle| &\leq \|(x, y, \theta)\| \cdot \|f(x, y, \theta, u)\| \\ &\leq \frac{1}{2} \|f(x, y, \theta, u)\| \left(1 + \|(x, y, \theta)\|^2\right) \\ &\leq \frac{1}{2} V(\theta)^2 \left(1 + \frac{1}{R(\theta)^2}\right) \left(1 + \|(x, y, \theta)\|^2\right) \\ &\leq C \left(1 + \|(x, y, \theta)\|^2\right), \end{aligned}$$

where $C = \max_{\theta \in S^1} \{ \frac{1}{2} V(\theta)^2 \left(1 + \frac{1}{R(\theta)^2}\right) \}$. Note that the maximum exists since $V(\theta)$ is bounded and $R(\theta) > 0$ for closed set S^1.

Section 2.2 established that for any given starting vehicle configuration (x_s, y_s, θ_s) and any given destination configuration (x_t, y_t, θ_t) there exists an admissible trajectory from (x_s, y_s, θ_s) to (x_t, y_t, θ_t).

Consequently, from Filippov's theorem we conclude the existence of an optimal path for any given starting and target states of the system.

2.4 Necessary Conditions for Optimality

We now derive the necessary conditions for optimality using Pontryagin's Minimum Principle (PMP) (Pontryagin et al., 1962). Let $\psi = (\psi_0(t), \psi_1(t), \psi_2(t), \psi_3(t))$ be the adjoint variables corresponding to $(x_0(t), x(t), y(t), \theta(t))$. We find the Hamiltonian $H(\psi, x_0, x, y, \theta, u) := \langle \psi, \mathbf{f} \rangle$ where $\mathbf{f} := (f_0, f_1, f_2, f_3)'$.

$$H = \psi_0 + \psi_1 V(\theta) \cos(\theta) + \psi_2 V(\theta) \sin(\theta) + \psi_3 \frac{V(\theta)}{R(\theta)} u, \tag{9}$$

and the adjoint system,

$$\begin{aligned}
\dot{\psi}_0 &= -\partial H/\partial x_0 = 0, && (10)\\
\dot{\psi}_1 &= -\partial H/\partial x = 0, && (11)\\
\dot{\psi}_2 &= -\partial H/\partial y = 0, && (12)\\
\dot{\psi}_3 &= -\partial H/\partial \theta = \psi_1 V(\theta)\sin(\theta) - \psi_1 V'(\theta)\cos(\theta) - \psi_2 V(\theta)\cos(\theta) && (13)\\
&\quad -\psi_2 V'(\theta)\sin(\theta) + \psi_3 \frac{V(\theta)R'(\theta)}{R(\theta)^2}u - \psi_3 \frac{V'(\theta)}{R(\theta)}u,
\end{aligned}$$

where $V'(\theta) = dV(\theta)/d\theta$ and $R'(\theta) = dR(\theta)/d\theta$.

Then ψ_0, ψ_1 and ψ_2 are constant on $[0, T]$. Similarly to Boissonnat et al. (1994), we simplify the notation by setting $\psi_1 = \lambda\cos(\phi)$ and $\psi_2 = \lambda\sin(\phi)$, where $\lambda = \sqrt{\psi_1^2 + \psi_2^2} \geq 0$ and $\phi < 2\pi$ such that $\tan(\phi) = \psi_2/\psi_1$.

We rewrite the Hamiltonian and $\dot{\psi}_3$ as follows,

$$\begin{aligned}
H &= \psi_0 + \lambda V(\theta)\cos(\theta - \phi) + \psi_3 \frac{V(\theta)}{R(\theta)}u, && (14)\\
\dot{\psi}_3 &= \lambda V(\theta)\sin(\theta - \phi) - \lambda V'(\theta)\cos(\theta - \phi) + \psi_3 \frac{V(\theta)R'(\theta)}{R(\theta)^2}u - \psi_3 \frac{V'(\theta)}{R(\theta)}u. && (15)
\end{aligned}$$

From PMP we know that if $u^*(t)$ is an optimal control function, then for all $t \in [0, T]$ we have

$$u^*(t) = \arg\min_{u\in[-1,1]} \left\{ \psi_0 + \lambda V(\theta(t))\cos(\theta(t) - \phi) + \psi_3(t)\frac{V(\theta(t))}{R(\theta(t))}u \right\}. \quad (16)$$

Furthermore, we know that for all $t \in [0, T]$

$$\psi_0 + \lambda V(\theta)\cos(\theta - \phi) + \psi_3 \frac{V(\theta)}{R(\theta)}u^* = 0, \quad (17)$$

and

$$\psi_0 \geq 0. \quad (18)$$

Then, for an optimal control u^*, along any $\mathcal{C}^2$ piece of the optimal path, we have

$$\psi_3 \frac{V(\theta)}{R(\theta)}u \leq 0. \quad (19)$$

Employing Assumptions 2 and 3, we simplify (19) as follows:

$$\psi_3 u \leq 0. \quad (20)$$

Furthermore, along any $\mathcal{C}^2$ piece of an optimal path either one of the following two cases holds (Boissonnat et al., 1994):

1. $\partial\mathbf{H}/\partial\mathbf{u} \equiv \mathbf{0}, \forall \mathbf{t} \in [\mathbf{t_1}, \mathbf{t_2}], \mathbf{t_1} < \mathbf{t_2}$, which implies $\psi_3 V(\theta)/R(\theta) \equiv 0$. Since $V(\theta) > 0, \forall\theta \in S^1$ and $R(\theta)$ is bounded, we know $\psi_3 = 0, \forall t \in [t_1, t_2]$. Then $\dot{\psi}_3 \equiv 0$, implying $\lambda V(\theta)\sin(\theta - \phi) - \lambda V'(\theta)\cos(\theta - \phi) = 0$ (see (15)).

Note that $\lambda \neq 0$, otherwise $\psi_1 = \psi_2 = 0$, and (14) would imply that $\psi_0 = 0$. However, PMP does not permit the vector ψ to be zero. Then, employing a calculus technique of taking the derivative of $V(\theta)$ in polar coordinate system (e.g., Youse (1978, pg. 676)) we obtain $V'(\theta) = V(\theta)\cot(\varphi(\theta))$, where $\varphi(\theta)$ is an angle between the tangent and radial lines of the $V(\theta)$ polar plot (i.e., equivalent to Cartesian plot of $V(\theta)(\cos(\theta), \sin(\theta))$ for $\theta \in [0, 2\pi]$). See Figure 3.

Solving the equation $\dot{\psi}_3 = 0$, we obtain

$$\varphi(\theta) + \theta = \phi \pm \frac{\pi}{2}. \quad (21)$$

Note that $\varphi(\theta) + \theta$ is the slope of the line tangent to the speed polar plot. Setting this angle to

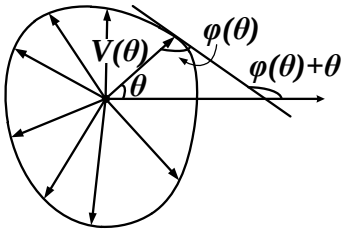

Figure 3: $\varphi(\theta)$ denotes an angle between the tangent and radial lines of the $V(\theta)$ polar plot.

constant ϕ corresponds to a straight line path with a fixed heading angle equal to θ.

2. Otherwise, $\partial \mathbf{H}/\partial \mathbf{u} \neq \mathbf{0}, \forall \mathbf{t} \in [\mathbf{t_1}, \mathbf{t_2}], \mathbf{t_1} < \mathbf{t_2}$, implying $\psi_3(t)V(\theta(t))/R(\theta(t)) \neq 0 \ \forall t$, then (16) states that $u^* = \pm 1$ corresponding to the sharpest possible turn.

By applying PMP we can state the following proposition.

Proposition 4. *Any optimal path is the concatenation of the arcs with minimum turning radius $R(\theta)$ and the straight line segments all parallel to the fixed directions defined by (21). Due to the general form of $V(\theta)$, there could be multiple distinct headings defined by equation (21).*

We would like to emphasize that we make no assumptions about the structure of the minimum turning radius function $R(\theta)$ and the speed function $V(\theta)$, and Proposition 4 is applicable to the general direction-dependent environment.

3 Further Analysis of an Optimal Path Structure

In the previous section, we demonstrated the controllability of our problem, proved the existence of an optimal path and derived the necessary conditions for optimality stated in Proposition 4. While Pontryagin's Principle provides important information about the structure of an optimal path, the derived results are only *necessary* conditions for optimality and therefore define a large set of potential optimal paths. In this section, we present further analysis of an optimal path structure and characterize a more specific set of optimal path candidates, which is significantly smaller.

In Section 3.1, we introduce the terminology and notation to be used throughout the paper. Section 3.2 lists general observations and properties that follow directly from the definitions and control model of the problem. These statements are used extensively in the corresponding proofs and provide a more intuitive understanding of the analysis. Section 3.3 describes the detailed analysis and resulting characterization of an optimal path for a general polar plot of the agent's speed function. In this section, we divide a path into a set of segments, establish the individual properties for those segments, and assemble the path segments into an optimal path. In Section 3.4 we consider a special case of the problem, where speed polar plot set is convex. This assumption allows us to further specify an optimal path structure and deliver Algorithm 1 that demonstrates the construction of such path (Section 3.5).

3.1 Terminology and Notation

- *Right-hand (left-hand) sharpest turn curve* - a continuous curve in $\mathbb{R}^2$ corresponding to a clockwise (counterclockwise) turn of the vehicle with the minimum turning radius, i.e., $u(t) = -1$ ($u(t) = 1$) in equation (3) (see Figure 4).

- $\mathcal{C}_R(\theta_1, \theta_2)$ ($\mathcal{C}_L(\theta_1, \theta_2)$) - a continuous segment (i.e., arc) of the right-hand (left-hand) sharpest turn curve that starts at the heading angle θ_1, ends at the angle θ_2, and spans an interval of headings smaller than 2π (i.e., the vehicle does not make the complete 2π turn). The curve is defined for $\theta_1, \theta_2 \in S^1$. Consequently, if $\theta_2 > \theta_1$ for $\mathcal{C}_R(\theta_1, \theta_2)$ we assume that the curve ends at the angle $\theta_2 - 2\pi$, and if $\theta_1 > \theta_2$ for $\mathcal{C}_L(\theta_1, \theta_2)$ we assume that the curve ends at the angle $\theta_2 + 2\pi$. See Figure 5.

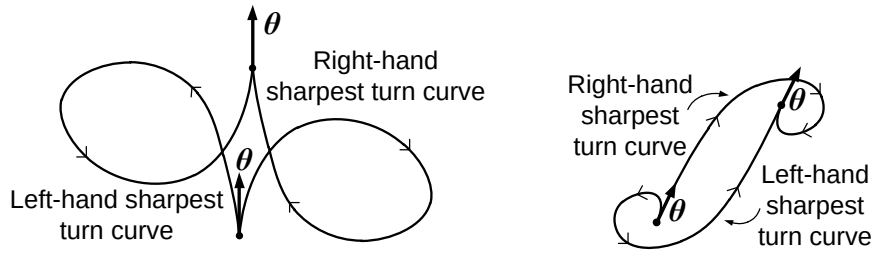

Figure 4: Examples of right-hand and left-hand sharpest turn curves. Note that a sharpest turn curve making a complete 2π turn does not necessarily end at its starting point.

When the actual direction of the curve has no significant value to a statement, we write $\mathcal{C}.(\theta_1, \theta_2)$ to denote a sharpest turn curve representing either $\mathcal{C}_R(\theta_1, \theta_2)$ or $\mathcal{C}_L(\theta_1, \theta_2)$.

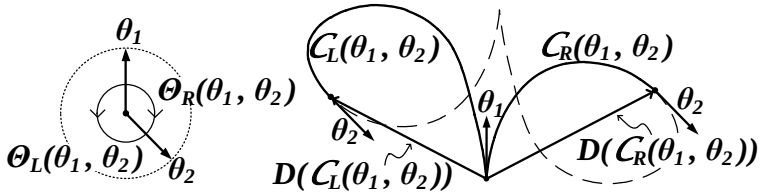

Figure 5: Polar plot of $\Theta_R(\theta_1, \theta_2)$ and $\Theta_L(\theta_1, \theta_2)$, and the corresponding curves $\mathcal{C}_R(\theta_1, \theta_2)$ and $\mathcal{C}_L(\theta_1, \theta_2)$.

- $\mathcal{C}_{.,2\pi}(\theta_1)$ - a sharpest turn curve that makes a complete 2π turn and starts (as well as ends) at the heading angle θ_1 (see Figure 4 for examples). We often refer to the curve as a 2π-*curve*.
- $\Theta_R(\theta_1, \theta_2)$ ($\Theta_L(\theta_1, \theta_2)$) - the set of all headings taken by an agent traversing a right-hand (left-hand) sharpest turn curve $\mathcal{C}_R(\theta_1, \theta_2)$ ($\mathcal{C}_L(\theta_1, \theta_2)$) as shown in Figure 5. Since the heading angle cannot be changed instantaneously, it is natural for the set of spanned angles to be a continuous interval of heading angles. For consistency, assume that $\Theta_R(\theta_1, \theta_2) \bigcup \Theta_L(\theta_1, \theta_2) \subseteq S^1$. Consequently,

$$\Theta_R(\theta_1, \theta_2) := \begin{cases} [\theta_2, \theta_1], & \text{if } \theta_1 > \theta_2 \\ [0, \theta_1] \cup [\theta_2, 2\pi), & \text{if } \theta_2 > \theta_1 \\ \theta_1 & \text{if } \theta_1 = \theta_2 \end{cases}, \text{ and}$$

$$\Theta_L(\theta_1, \theta_2) := \begin{cases} [\theta_1, \theta_2], & \text{if } \theta_1 < \theta_2 \\ [0, \theta_2] \cup [\theta_1, 2\pi), & \text{if } \theta_2 < \theta_1 \\ \theta_1 & \text{if } \theta_1 = \theta_2 \end{cases}.$$

- $\|\Theta_k(\theta_1, \theta_2)\|$ - size of the set $\Theta_k(\theta_1, \theta_2)$ ($k \in \{R, L\}$), which is equal to the sum of the lengths of the angle intervals belonging to the set.
- $D(.)$ - a displacement vector (from the start point to the end point) for a path given as an input. For example, $D(\mathcal{C}_R(\theta_1, \theta_2))$ denotes the displacement vector corresponding to a curve $\mathcal{C}_R(\theta_1, \theta_2)$, see Figure 5.
  A shorthand notation D_{st} denotes the displacement vector from the starting point (x_s, y_s) to the destination point (x_t, y_t), that is $D_{st} := (x_t, y_t) - (x_s, y_s)$.
- $\alpha(.)$ - a heading angle of a vector specified as an input. For examples $\alpha(D_{st})$ denotes the angle of the displacement vector D_{st}.

- $\tau(.)$ - a travel time function that returns the total travel time along a path specified as an input. For example, $\tau(\mathcal{C}_R(\theta_1, \theta_2))$ denotes the travel time along a curve $\mathcal{C}_R(\theta_1, \theta_2)$.
  The value of the travel time function can be computed as follows:
  - for sharpest turn curve $\mathcal{C}_k(\theta_a, \theta_b)$ where $k \in \{R, L\}$, $\tau(\mathcal{C}_k(\theta_a, \theta_b)) = \left| \int_{\Theta_k(\theta_a, \theta_b)} \frac{R(\theta)}{V(\theta)} d\theta \right|$,
  - for straight line segment from $a = (x_a, y_a)$ to $b = (x_b, y_b)$, denoted by S_{ab}, $\tau(S_{ab}) = \frac{||\vec{ab}||}{V(\alpha(S_{ab}))}$.
- $(x_R, y_R) := (x_s, y_s) + D(\mathcal{C}_R(\theta_s, \theta_t))$ - the end point of a right-hand sharpest turn curve $\mathcal{C}_R(\theta_s, \theta_t)$ that starts at point (x_s, y_s), see Figure 6.
- $(x_L, y_L) := (x_s, y_s) + D(\mathcal{C}_L(\theta_s, \theta_t))$ - the end point of a left-hand sharpest turn curve $\mathcal{C}_L(\theta_s, \theta_t)$ that starts at point (x_s, y_s), see Figure 6.

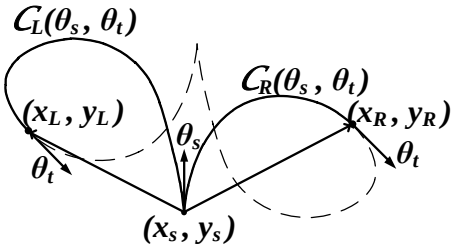

Figure 6: Definition of (x_R, y_R) and (x_L, y_L).

- *(Time) reversed curve* of a specified curve - a curve that spans the same set of headings but in the reversed order. For example, curve $\mathcal{C}_L(\theta_2, \theta_1)$ is the (time) reversed curve of (or corresponding to) $\mathcal{C}_R(\theta_1, \theta_2)$, see Figure 10.
- *Time reversed path* - a path corresponding to a specified heading angle sequence traversed in reverse order. This is a generalization of a *time reversed curve*.
- θ^u_{ab}, θ^d_{ab} - two heading angles such that, for any given points a and b, the line segment connecting the points $(\theta^u_{ab}, V(\theta^u_{ab}))$ and $(\theta^d_{ab}, V(\theta^d_{ab}))$ (in polar coordinates) corresponds to the boundary of a set enclosed by the convex hull of the speed polar plot centered at point a, and this line segment intersects the half-line $[a, b)$. Furthermore, we let $\theta^u_{ab} \in (\alpha(D(b-a)), \alpha(D(b-a)) + \pi)$ and $\theta^d_{ab} \in (\alpha(D(b-a)) - \pi, \alpha(D(b-a)))$ (see Figure 7). In other words, these angles are such that following a segment with heading θ^u_{ab} and then a segment with heading θ^d_{ab} would yield a fastest path from a to b if we did not have any minimum turning radius constraint. Note that for a given speed function $V(\theta)$, θ^u_{ab} and θ^d_{ab} only depend on the heading angle of the vector $\overrightarrow{ab}$ and not the actual points a and b. The presented notation is specifically chosen for the ease of discussion later in the paper. The angles θ^u_{ab} and θ^d_{ab} may not be unique and we thus let $\mathcal{U}(a, b)$ and $\mathcal{D}(a, b)$ be the sets of all such θ^u_{ab} and θ^d_{ab}, respectively. For the headings where the speed polar plot and the convexified speed polar plot coincide, we have $\theta^u_{ab} = \theta^d_{ab} = \alpha(D(b-a))$. More detailed discussion of these angles and their properties can be found in (Dolinskaya & Smith, 2012).
- D^u_{ab}, D^d_{ab} - two line segments such that $\alpha(D^u_{ab}) = \theta^u_{ab} \in \mathcal{U}(a, b)$, $\alpha(D^d_{ab}) = \theta^d_{ab} \in \mathcal{D}(a, b)$ and $a + D^u_{ab} + D^d_{ab} = b$. Note that such D^d_{ab} and D^u_{ab} may not be unique, yet for a given speed function, the total travel time along any $D^u_{ab} + D^d_{ab}$ is the same, and we select one such pair of D^u_{ab}, D^d_{ab} arbitrarily. (See Figure 7.)

3.2 Some General Observations and Properties

This section provides general observations and properties for the sharpest turn curves and displacement vectors defined above. These observations and properties provide an intuitive understanding of the

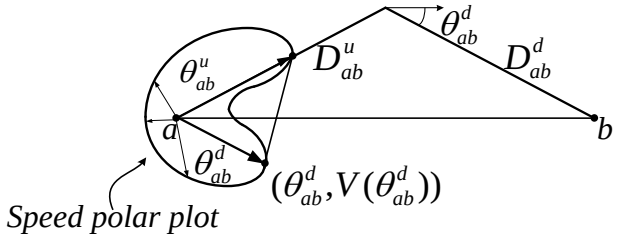

Figure 7: Illustration of the notations $\theta^u_{ab}, \theta^d_{ab}, D^u_{ab}$ and D^d_{ab}

problem structure and a foundation for further analysis of the optimal path. The listed properties are direct derivations from the problem statement and the control model established in equations (1)-(4), the proofs are straightforward calculus exercises and are therefore omitted.

Property 5. *In the case where there is no constraint on the minimum turning radius (i.e., $R(\theta) = 0$, $\forall\theta \in S^1$), the smallest travel time from $a \in \mathbb{R}^2$ to $b \in \mathbb{R}^2$ is given by $\tau(D^u_{ab}) + \tau(D^d_{ab})$. Consequently, $\tau(D^u_{ab}) + \tau(D^d_{ab})$ represents a lower bound on the travel time from a to b. (See (Dolinskaya* et al.*, 2009) for proof.)*

Observation 6. *For any $\theta_1, \theta_2 \in S^1$, the minimum turning radius function $R(\theta)$ uniquely characterizes the right-hand and left-hand sharpest turn curves $\mathcal{C}_R(\theta_1, \theta_2)$ and $\mathcal{C}_L(\theta_1, \theta_2)$.*

Observation 7. *The speed function $V(\theta)$ describes how fast a vehicle moves along a sharpest turn curve (or any other path); that is, $V(\theta)$ uniquely characterizes the functional τ.*

The following three propositions establish the relationship between the sharpest turn curves and their corresponding displacement. Note that unlike the Dubins car problem where such curves correspond to arcs of a circle with fixed radius, we cannot compute the precise displacement along a sharpest turn curve without the explicit expression for $R(\theta)$. Thus, the propositions establish only limited properties that hold true for our general problem.

Property 8. *The slope of a displacement vector for an arbitrary curve must belong to the set of all the headings taken by a vehicle traversing that curve, provided the size of the spanned angles set is less than or equal to π. Mathematically, for some θ_1 and θ_2, $\alpha(D(\mathcal{C}_k(\theta_1, \theta_2))) \in \Theta_k(\theta_1, \theta_2)$ if $||\Theta_k(\theta_1, \theta_2)|| \leq \pi$, where $k \in \{R, L\}$. (See $\mathcal{C}_R(\theta_1, \theta_2)$ on Figure 5 for an example.)*

Property 9. *Consider an arbitrary curve $\mathcal{C}_k(\theta_1, \theta_2)$ with $||\Theta_k(\theta_1, \theta_2)|| \leq \pi$ for $k \in \{R, L\}$ and the following two lines: l_1 passing through the start point of the curve with the slope θ_1, and l_2 passing through the end point of the curve with slope θ_2. The curve $\mathcal{C}_k(\theta_1, \theta_2)$ does not intersect l_1 and l_2 except for its start and end points, respectively.*

Furthermore, if $\Theta_k(\theta_1, \theta_2) < \pi$, the curve lies inside the triangle region bounded by lines l_1, l_2 and $D(\mathcal{C}_k(\theta_1, \theta_2))$ as shown by Figure 8.

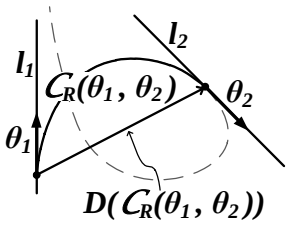

Figure 8: Illustration of Property 9.

Property 10. *A sharpest turn curve $\mathcal{C}_k(\theta_1, \theta_2)$ with $||\Theta_k(\theta_1, \theta_2)|| > \pi$ for $k \in \{R, L\}$ can have at most one point of intersection with itself. Furthermore, the heading angle of its displacement vector $\alpha(D(\mathcal{C}_k(\theta_1, \theta_2))) \notin \Theta_k(\theta_1, \theta_2)$ only if the curve has an intersection point with itself. And $\alpha(D(\mathcal{C}_k(\theta_1, \theta_2))) \in \Theta_k(\theta_1, \theta_2)$ if the curve $\mathcal{C}_k(\theta_1, \theta_2)$ does not have a point of intersection, see Figure 9.*

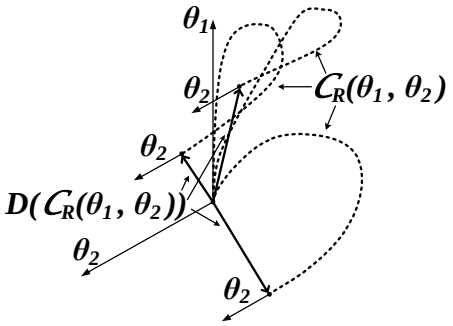

Figure 9: Illustration of the possible sharpest turn curves as described in Property 10.

Property 11. *The travel times and the displacement vectors for a pair of time reversed curves are equal to each other. That is, $\tau(\mathcal{C}_R(\theta_1, \theta_2)) = \tau(\mathcal{C}_L(\theta_2, \theta_1))$ and $D(\mathcal{C}_R(\theta_1, \theta_2)) = D(\mathcal{C}_L(\theta_2, \theta_1))$ for arbitrary $\theta_1, \theta_2 \in S^1$, see Figure 10. More generally, the travel times and displacement vectors are the same for a pair of paths that are time reversed of each other.*

For an intuitive proof of Proposition 11, note that the displacement and travel time functions can be expressed as integration over the (same) set of spanning heading angles, since $\Theta_R(\theta_1, \theta_2) = \Theta_L(\theta_2, \theta_1)$.

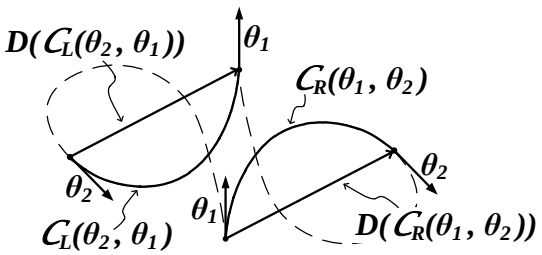

Figure 10: Illustration of $\mathcal{C}_R(\theta_1, \theta_2)$ and $\mathcal{C}_L(\theta_2, \theta_1)$ properties.

Property 12. *The travel time and displacement vector are the same for a 2π-curve regardless of the starting heading angle. That is, $\tau(\mathcal{C}_{.,2\pi}(\theta_1)) = \tau(\mathcal{C}_{.,2\pi}(\theta_2))$ and $D(\mathcal{C}_{.,2\pi}(\theta_1)) = D(\mathcal{C}_{.,2\pi}(\theta_2))$ for any θ_1 and θ_2 as shown by Figure 11.*

Since the travel time $\tau(.)$ and the displacement vector $D(.)$ are equivalent for the right-hand and left-hand 2π sharpest turn curves (Property 11), as well as for any pair of starting heading angles (Property 12), we can simplify our notation.

- $\tau(C_{2\pi}) := \tau(\mathcal{C}_{.,2\pi}(\theta_1)),\ \forall \theta_1 \in S^1$.
- $D(C_{2\pi}) := D(\mathcal{C}_{.,2\pi}(\theta_1)),\ \forall \theta_1 \in S^1$.

Property 13. *Consider a given path, which is arbitrarily divided into a set of segments. Due to the additive property of time and displacement, the total travel time and the total displacement vector for the given path are equal to the sum of travel times and displacements for the path segments, respectively.*

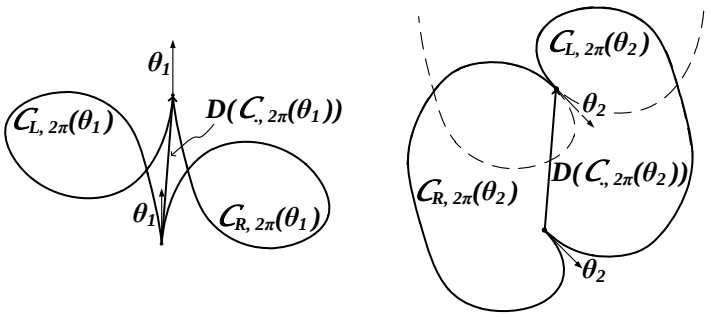

Figure 11: Properties of $\tau(\mathcal{C}_{\cdot,2\pi}(\theta_1))$ and $D(\mathcal{C}_{\cdot,2\pi}(\theta_1))$.

Property 14. *Consider an arbitrary feasible path divided into a finite number of path segments which are then arbitrarily rearranged into an alternative continuous path. Time and space homogeneous properties of the functions $R(\theta)$ and $V(\theta)$ and Property 13 imply that the rearranged path has the same total travel time and displacement vector as the original path.*

Note that a path obtained by rearranging finite number of segments of a feasible path that satisfies the minimum turning radius constraint is likely not to be feasible, since the turning constraints may be violated at the points joining two path segments. The segmentation and rearrangement process of a feasible path is only a thought process used throughout the paper to ease the discussion and to establish the key properties of an optimal path. Thus, we introduce a *relaxation* of our original fastest-path problem by relaxing the feasibility constraint of minimum turning radius at a finite number of points along a path. We define a *relaxed-feasible* path to be a path such that it can be partitioned into a finite number of segments, which can be rearranged into a feasible path (i.e., satisfying minimum turning radius constraint along its entire length). See Figure 16 for an example of a *relaxed-feasible* path and its rearrangement into a feasible path. Then, a *relaxed-optimal* path is a path that can be rearranged into optimal path for our original problem. Similarly, we use the term *feasible transformation* to denote a transformation (rearrangement or substitution of path segments) of one *relaxed-feasible* path into another *relaxed-feasible* path, i.e., maintaining the property that the newly transformed path can still be rearranged into a feasible path.

Observation 15. *When an optimal path has two segments with the same displacement and one of the components can be replaced by the other without violating the minimum turning radius constraint, the travel time along the two components must be the same.*

Indeed, if it was not the case, we could substitute the slower component by the faster one to yield a faster path.

Property 14 and Observation 15 are instrumental in the forthcoming discussion of an optimal path that establishes certain properties of the path segments and then arranges them into a single fastest path.

3.3 Structure of the optimal path

In this section, we analyze the structure of an optimal path for a general speed function $V(\theta)$ subject to a minimum turning radius constraint given by the general function $R(\theta)$ for $\theta \in S^1$. Note that $V(\theta)$ might correspond to a non-convex polar plot, in which case traveling along the shortest path (e.g., straight line segment) can be suboptimal. The objective is to derive results akin to those found in the Dubins car problem but with a larger class of applications since we relax a number of constraints. Indeed, the Dubins car problem concerns a vehicle with constant turning radius and constant speed while the problem tackled in this paper does not make such restrictions. Thus, Dubins car problem is a special case of our problem.

Before delving in the analysis of the optimal path structure, consider a simple example illustrated in Figure 12 in order to gain intuition as to the changes brought by the relaxation of the constant turning

radius and speed assumptions.

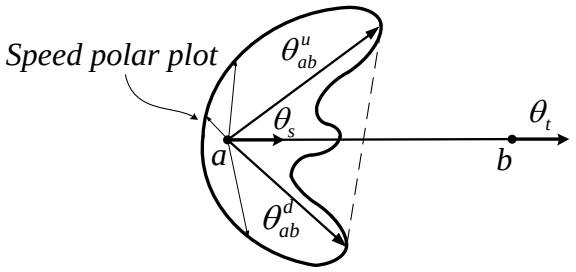

Figure 12: Example of a non-convex speed polar plot.

Suppose we want to travel from $a \in \mathbb{R}^2$ to $b \in \mathbb{R}^2$ where the initial and final headings are the same and borne by the vector $\vec{ab}$. In the absence of minimum turning radius constraint, a shortest path is found by a combination of straight line segments with headings θ^u_{ab} and θ^d_{ab} (Property 5). Similarly, if we do include the minimum radius constraint and b is far enough from a, the optimal path is to turn as sharply as possible to the heading angle θ^u_{ab}, follow a straight line, then turn to the heading angle θ^d_{ab}, follow a straight line before coming back to the original heading. However, if b is relatively close to a, we simply want to follow a straight segment from a to b since the cost of making turns would not be compensated by the potential savings achieved while traveling along θ^u_{ab} and θ^d_{ab}. Thus, in the case of a non-convex speed polar plot, where a straight line is no longer the fastest path, we need to take into account the trade-off between using the headings with better speed values and the time it takes to reach those heading angles by following the sharpest turn curves. In Section 4 we demonstrate an application of our results to a vessel routing problem, which provides another illustration.

3.3.1 Preliminary analysis of an optimal path structure

In order to establish our key results, we first state some preliminary results that serve as tools to build the desired properties.

We have already derived through optimal control theory results (Proposition 4) that the optimal path consists of a combination of straight lines and sharpest possible turns. We wish to go further and establish a more precise result. In order to do so, we divide the path into segments that are easier to analyze, and state properties that they must individually satisfy so that the path remains feasible and their aggregation is optimal, i.e., together, the segments correspond to *relaxed-optimal* path. Thus, the analysis that follows divides the path into a set of easy-to-analyze segments, establishes the individual properties for those segments that guarantees feasibility and optimality of the aggregated path, and then assembles the path segments into an optimal path from (x_s, y_s, θ_s) to (x_t, y_t, θ_t).

To begin, note that for a distinct pair of starting and target heading angles (i.e., $\theta_s \neq \theta_t$) we know that somewhere along an optimal path one has to traverse a right-hand or a left-hand sharpest turn curve from θ_s until θ_t. In other words, an optimal path must contain either $\mathcal{C}_R(\theta_s, \theta_t)$ or $\mathcal{C}_L(\theta_s, \theta_t)$, which may be split into a number of segments throughout the path (see Figure 13). (If $\theta_s = \theta_t$, we set $\mathcal{C}.(\theta_s, \theta_t) = \emptyset$ and follow the same discussion.)

Property 14 states that a path may be divided into segments that can be rearranged at will to facilitate their study. Hence, we extract all the pieces that are part of the necessary turn from θ_s to θ_t and consider the remaining pieces separately. Thus we divide an optimal path into a sharpest turn curve, either $\mathcal{C}_R(\theta_s, \theta_t)$ or $\mathcal{C}_L(\theta_s, \theta_t)$, and the remaining part of the path called a *sub-path*. Consequently, an optimal path from (x_s, y_s) to (x_t, y_t) corresponds to either one of the following two cases (see Figure 14):

1. contains the segments making up the curve $\mathcal{C}_R(\theta_s, \theta_t)$ and a *relaxed-optimal sub-path* from point (x_R, y_R) to (x_t, y_t), or
2. contains the segments making up the curve $\mathcal{C}_L(\theta_s, \theta_t)$ and a *relaxed-optimal sub-path* from point (x_L, y_L) to (x_t, y_t).

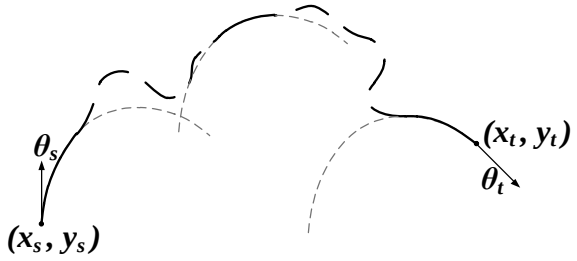

Figure 13: Conceptual example of an optimal path consisting of the segments making up the curve $\mathcal{C}_R(\theta_s, \theta_t)$ (solid bold lines) and the remaining segments making up the sub-path (dashed bold lines).

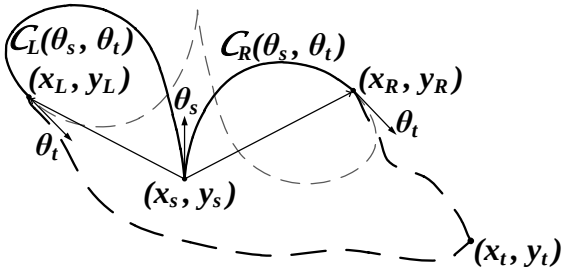

Figure 14: An optimal path can be broken down into a sharpest turn curve from θ_s until θ_t (bold solid lines) and the remaining sub-path (bold dashed lines).

Note that not every optimal path necessarily starts with $\mathcal{C}_k(\theta_s, \theta_t)$ for $k \in \{R, L\}$; we only state that the path has to be made up of the segments forming the curve $\mathcal{C}_k(\theta_s, \theta_t)$ and a set of path segments we called a *relaxed-optimal sub-path*. We define a *relaxed-optimal sub-path* to be a finite set of feasible path segment (each satisfying the minimum turning radius constraint) that, together with $\mathcal{C}_k(\theta_s, \theta_t)$ for $k \in \{R, L\}$, correspond to a *relaxed-optimal* path. Thus, when rearranging the segments of an optimal path into a sharpest turn curve $\mathcal{C}_k(\theta_s, \theta_t)$, the remaining segments are organized into a continuous sub-path from either (x_R, y_R) or (x_L, y_L) to (x_t, y_t), which may have points of discontinuous heading angles where the segments are joined together. Therefore, a sub-path is not necessarily feasible on its own (we are only concerned with feasibility of the reassembled path). We call it a *relaxed-optimal sub-path* to differentiate from the optimality defined earlier, which implies feasibility. Thus, a *relaxed-feasible sub-path* is a path that, together with the sharpest turn curve $\mathcal{C}_k(\theta_s, \theta_t)$ for $k \in \{R, L\}$, is a *relaxed-feasible* path as defined in Section 3.2. Then, we call a *relaxed-optimal sub-path* the minimum-travel time or fastest *relaxed-feasible sub-path*, since a *relaxed-feasible sub-path* is *relaxed-optimal* if and only if it is the fastest among all *relaxed-feasible sub-paths*. In the forthcoming characterization of a *relaxed-optimal sub-path* we analyze the structure of a sub-path that guarantees optimality of a reassembled path.

In a general setting, it is unknown a priori which of the two scenarios stated above is optimal (Figure 14). Therefore, we find the fastest paths corresponding to each case, and the path with smaller travel time is established to be optimal for our problem. To simplify the notation, we let D_{Rt} denote the displacement vector from (x_R, y_R) to (x_t, y_t), that is $D_{Rt} = D_{st} - D(\mathcal{C}_R(\theta_s, \theta_t))$, and let $D_{Lt} = D_{st} - D(\mathcal{C}_L(\theta_s, \theta_t))$.

3.3.2 Lower and upper bounds on minimum travel time from (x_s, y_s, θ_s) to (x_t, y_t, θ_t)

First, we find a lower bound on the minimum travel time when an optimal path has to contain segments making up a right-hand sharpest turn curve $\mathcal{C}_R(\theta_s, \theta_t)$; denote such bound by LB_R. The optimal path

corresponding to this case contains the curve $\mathcal{C}_R(\theta_s, \theta_t)$ and a *relaxed-optimal sub-path* from point (x_R, y_R) to point (x_t, y_t). From Property 5, we know that the fastest path from (x_R, y_R) to (x_t, y_t) in the absence of minimum turning radius constraint is given by $D^u_{Rt} + D^d_{Rt}$ where we let $D^u_{Rt} := D^u_{(x_R,y_R)(x_t,y_t)}$ and $D^d_{Rt} := D^d_{(x_R,y_R)(x_t,y_t)}$ to avoid cumbersome notations (see Figure 16). This gives us a lower bound on the travel time from (x_R, y_R) to (x_t, y_t). Therefore, a travel time along a *relaxed-optimal sub-path* from (x_R, y_R) to (x_t, y_t) cannot be less than the travel time along that path (note that only if $\exists \theta_u \in \mathcal{U}(R,t)$ and $\exists \theta_d \in \mathcal{D}(R,t)$ such that $\theta_u, \theta_d \in \Theta_R(\theta_s, \theta_t)$ could this path be rearranged into a feasible and therefore optimal path, see Proposition 16 and Figure 16). Consequently,

$$LB_R = \tau(\mathcal{C}_R(\theta_s, \theta_t)) + \tau(D^u_{Rt}) + \tau(D^d_{Rt}). \tag{22}$$

Analogously to the right-hand sharpest turn curve case, we find a lower bound on the minimum travel time when an optimal path has to contain segments making up a left-hand sharpest turn curve $\mathcal{C}_L(\theta_s, \theta_t)$. (The lower bound for this case is denoted by LB_L.)

$$LB_L = \tau(\mathcal{C}_L(\theta_s, \theta_t)) + \tau(D^u_{Lt}) + \tau(D^d_{Lt}). \tag{23}$$

Considering that an optimal path has to correspond to one of the two scenarios discussed above, we can conclude that the overall lower bound on the minimum travel time (denoted by LB) is the minimum of the two bounds. That is,

$$LB \quad = \quad \min\{LB_R; LB_L\}.$$

To find an upper bound on the minimum travel time, we construct a feasible path which may or may not be optimal. Consider a path containing a 2π-curve, either $\mathcal{C}_{R,2\pi}(.)$ or $\mathcal{C}_{L,2\pi}(.)$. Then, a straight line path with any heading is a feasible part of the path and can be inserted into the 2π-curve part of the path without violating the minimum turning radius constraint (see Figure 15). Consequently, in the case when an optimal path has to contain the right-hand turn curve $\mathcal{C}_R(\theta_s, \theta_t)$, a *relaxed-feasible sub-path* can consist of a 2π-curve and the straight line segments D^u_{Qt} and D^d_{Qt} connecting the point $Q := (x_R, y_R) + D(\mathcal{C}_{2\pi})$ to (x_t, y_t). This path provides an upper bound on the minimum travel time, denoted by UB_R.

$$UB_R = \tau(\mathcal{C}_R(\theta_s, \theta_t)) + \tau(\mathcal{C}_{2\pi}) + \tau(D^u_{Qt}) + \tau(D^d_{Qt}). \tag{24}$$

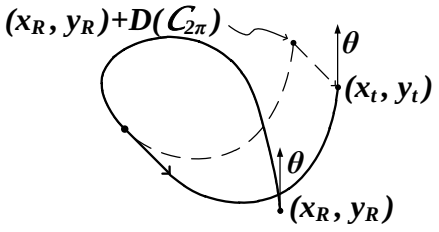

Figure 15: Example of a straight line segment inserted into a 2π-curve part of the path without violating the minimum turning radius constraint.

Similarly, we find an upper bound on the minimum travel time when an optimal path has to contain a left-hand sharpest turn curve $\mathcal{C}_L(\theta_s, \theta_t)$; we denote such bound by UB_L. (Here $\tilde{Q}$ is defined as $\tilde{Q} := (x_L, y_L) + D(\mathcal{C}_{2\pi})$.)

$$UB_L = \tau(\mathcal{C}_L(\theta_s, \theta_t)) + \tau(\mathcal{C}_{2\pi}) + \tau(D^u_{\tilde{Q}t}) + \tau(D^d_{\tilde{Q}t}). \tag{25}$$

Due to the fact that both of the constructed paths are feasible, the minimum of the two bounds delivers a tighter upper bound.

$$UB \quad = \quad \min\{UB_R; UB_L\}. \tag{26}$$

The constructed upper and lower bounds are used in our subsequent characterization of a *relaxed-optimal sub-path*.

3.3.3 Characterization of a *relaxed-optimal sub-path*

In order for a path from (x_s, y_s, θ_s) to (x_t, y_t, θ_t) to be optimal, a corresponding sub-path has to be a minimum travel-time path among the *relaxed-feasible sub-paths*. Therefore, we are interested in characterizing the minimum travel-time *relaxed-feasible sub-paths* from points (x_R, y_R) and (x_L, y_L) to the target point (x_t, y_t). By definition and construction, a *relaxed-feasible sub-path* has to satisfy a certain set of constraints to guarantee feasibility of a reassembled path, which are not explicitly defined at this point. As opposed to stating general and elaborate *relaxed-feasibility* constraints, we break our problem down into an exhaustive set of scenarios and discuss the constraints specific to each scenario as we consider them below.

It is important to note that in the case of the non-convex speed polar plot, the triangle inequality might not (and often does not) hold and the optimal solution might not be unique. In the following analysis we find only one of potentially infinitely many optimal paths and establish its optimality by proving that no other *relaxed-feasible sub-path* can have smaller travel time. The analysis of the two sub-path cases (starting at (x_R, y_R) and (x_L, y_L)) is practically identical, and without loss of generality, we limit our discussion to the case of a *relaxed-optimal sub-path* starting at point (x_R, y_R).

Scenario I: $\exists(\theta_u, \theta_d) \in \mathcal{U}(R,t) \times \mathcal{D}(R,t)$ **such that** $(\theta_u, \theta_d) \in \Theta_R(\theta_s, \theta_t)$

We first look at a special case of the problem where a *relaxed-optimal sub-path* can be concluded directly from the lower bound LB_R.

Proposition 16. *The sub-path consisting of* $D^u_{Rt} := D^u_{(x_R,y_R)(x_t,y_t)}$ *and* $D^d_{Rt} := D^d_{(x_R,y_R)(x_t,y_t)}$ *is a fastest* relaxed-feasible sub-path *if* $\exists(\theta_u, \theta_d) \in \mathcal{U}(R,t) \times \mathcal{D}(R,t)$ *such that* $(\theta_u, \theta_d) \in \Theta_R(\theta_s, \theta_t)$. *Then, a fastest path from* (x_s, y_s) *to* (x_t, y_t) *containing segments making up a right-hand sharpest turn is obtained by inserting the straight line segments* D^u_{Rt} *and* D^d_{Rt} *in the necessary curve* $\mathcal{C}_R(\theta_s, \theta_t)$ *(see Figure 16).*

Proof. We have established that the path consisting of D^u_{Rt} and D^d_{Rt} yields a theoretic lower bound on the travel time from (x_R, y_R) to (x_t, y_t). In the case where $\exists(\theta_u, \theta_d) \in \mathcal{U}(R,t) \times \mathcal{D}(R,t)$ such that $(\theta_u, \theta_d) \in \Theta_R(\theta_s, \theta_t)$ these segments can actually be inserted in the necessary curve $\mathcal{C}_R(\theta_s, \theta_t)$ to make a feasible path (see Figure 16). Since we have been able to insert a sub-path which attains its lower bound, it follows that we have thus constructed an optimal path. □

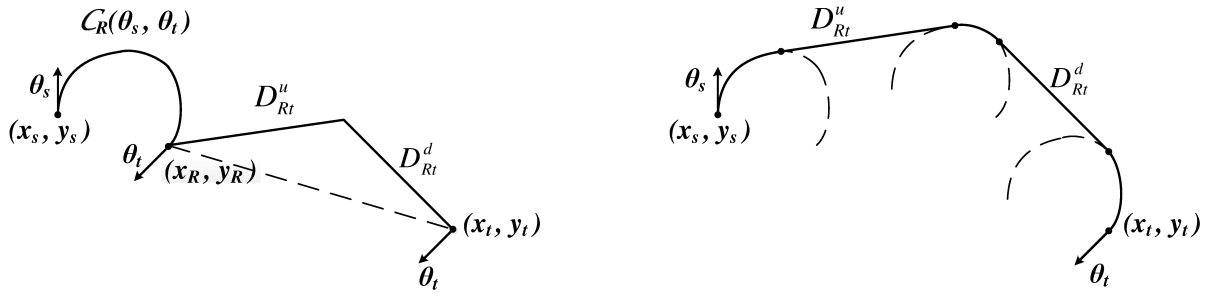

Figure 16: Illustration of two line segments (D^u_{Rt} and D^d_{Rt}) inserted into a necessary curve part of the path ($\mathcal{C}_R(\theta_s, \theta_t)$) without violating the minimum turning radius constraint.

Scenario II: $\nexists(\theta_u, \theta_d) \in \mathcal{U}(R,t) \times \mathcal{D}(R,t)$ **such that** $(\theta_u, \theta_d) \in \Theta_R(\theta_s, \theta_t)$

We now suppose that the turn $\mathcal{C}_R(\theta_s, \theta_t)$ does not contain both $\theta_u \in \mathcal{U}(R,t)$ and $\theta_d \in \mathcal{D}(R,t)$, and we cannot readily insert two straight lines into the necessary curve as in the first scenario. Consequently, there might be additional turns and straight lines to be made in the sub-path. However, an important observation due to the fact that the necessary change in heading is already realized by $\mathcal{C}_R(\theta_s, \theta_t)$ is that the total heading change of the *relaxed-optimal sub-path* must be 0 mod 2π.

We then distinguish two cases, one where the *relaxed-optimal sub-path* contains a 2π curve (possibly split into several segments) and one where it does not.

Scenario II (a): $\nexists(\theta_u, \theta_d) \in \mathcal{U}(R,t) \times \mathcal{D}(R,t)$ **such that** $(\theta_u, \theta_d) \in \Theta_R(\theta_s, \theta_t)$ **and a sub-path contains a** 2π**-curve.** The portion of the *relaxed-optimal sub-path* we now consider is the one joining $(x_Q, y_Q) := (x_R, y_R) + D(\mathcal{C}_{2\pi})$ to (x_t, y_t). As stated previously, a lower bound on the travel time from (x_Q, y_Q) to (x_t, y_t) is given by $\tau(D^u_{Qt}) + \tau(D^d_{Qt})$ where $D^d_{Qt} := D^d_{(x_Q, y_Q)(x_t, y_t)}$ and $D^u_{Qt} := D^u_{(x_Q, y_Q)(x_t, y_t)}$. Because of the 2π-curve, we are guaranteed that we are able to include the straight line segments D^d_{Qt} and D^u_{Qt} with headings $\theta_u \in \mathcal{U}(Q,t)$ and $\theta_d \in \mathcal{D}(Q,t)$, thus making an optimal path in a similar fashion to Scenario I.

Proposition 17. *In the case when* $\nexists(\theta_u, \theta_d) \in \mathcal{U}(R,t) \times \mathcal{D}(R,t)$ *such that* $(\theta_u, \theta_d) \in \Theta_R(\theta_s, \theta_t)$*, and a sub-path contains a* 2π*-curve, the remaining segment of the path consisting of* D^u_{Qt} *and* D^d_{Qt} *corresponds to a fastest* relaxed-feasible sub-path*. Then, a fastest path from* (x_s, y_s) *to* (x_t, y_t) *containing segments making up the right-hand sharpest turn is obtained by inserting the straight line segments* D^u_{Qt} *and* D^d_{Qt} *in the* 2π*-curve* $\mathcal{C}_{R,2\pi}(\theta_t)$*.*

Scenario II (b): $\nexists(\theta_u, \theta_d) \in \mathcal{U}(R,t) \times \mathcal{D}(R,t)$ **such that** $(\theta_u, \theta_d) \in \Theta_R(\theta_s, \theta_t)$ **and a sub-path does not contain a** 2π**-curve.** Scenarios I and II (a) are easy in the sense that we can readily insert the desired straight lines into the path in order to make it optimal. Scenario II (b) is more complicated.

Since a *relaxed-optimal sub-path* might not be unique, we are interested in characterizing only one of the *relaxed-optimal sub-path*s from (x_R, y_R) to (x_t, y_t). We prove a set of propositions where each consecutive statement adds more details to the structure of a *relaxed-optimal sub-path* without violating the preceding propositions. As a result, we obtain a specific structure of a sub-path known to be *relaxed-optimal*. Recall that from the earlier findings derived from optimal control theory analysis in Section 2 and summed up in Proposition 4, we already know that an optimal path consists of sharpest turns and straight lines.

Proposition 18. *There exists a* relaxed-optimal sub-path *with at most 2 straight line segments. That is, any optimal path with more than two straight line segments with distinct headings can be changed by feasible transformations into an optimal path with at most two straight line segments.*

Proof. Consider a *relaxed-feasible sub-path* which contains three line segments L_1, L_2 and L_3 with distinct headings. Consider the total displacement $D(L_1 + L_2 + L_3)$ realized by the three segments and set this direction as the x-axis (see Figures 17 and 18). In this new coordinate system, let $\theta_1, \theta_2, \theta_3 \in S^1$ be the respective heading angles of the three straight line segments L_1, L_2 and L_3. Since the total displacement lies on the x-axis, we must have at least one of the angles belonging to $[0, \pi)$ and another one to $[\pi, 2\pi)$. Assume, without loss of generality, that θ_1, θ_2 are in $[0, \pi)$ and θ_3 in $[\pi, 2\pi)$.

We consider the path obtained by following L_1, then L_2 and L_3. We let a and b be the extremities of L_1, b and c those of L_2, and c and d those of L_3. We then break down the proof into two distinct cases: (i) $\|\Theta_R(\theta_1, \theta_3)\| < \pi$ (Figure 17) and (ii) $\|\Theta_R(\theta_1, \theta_3)\| \geq \pi$ (Figure 18).

(i) $\|\Theta_R(\theta_1, \theta_3)\| < \pi$**:** See Figure 17. We define e as the intersection of the lines bearing L_1 and L_3, g be the intersection of L_3 and the line passing through a and parallel to L_2, and f be the intersection of ag and the line passing through b and parallel to L_3.

The original path is $abcd$, and we seek to replace it by a path at least as fast but containing at most two line segments. Because $\theta_1 - \theta_3 < \pi$, $\triangle aed$ forms a triangle containing L_1 and L_3. Using segments parallel to L_2 and L_3, we observe that the triangles $\triangle bec$ and $\triangle abf$ are similar. Since the triangles are similar, we have $\frac{\|be\|}{\|ab\|} = \frac{\|bc\|}{\|af\|} = \frac{\|ec\|}{\|bf\|} =: \alpha$. As a result, the travel times along

each of the edges share the same proportionality relation: $\frac{\tau(be)}{\tau(ab)} = \frac{\|be\|/V(\theta_1)}{\|ab\|/V(\theta_1)} = \alpha$ and so on. In particular, we have:

$$\frac{\tau(be)+\tau(ec)}{\tau(bc)} = \frac{\tau(ab)+\tau(bf)}{\tau(af)} =: \beta.$$

Then, if $\beta < 1$, the travel time along bc is greater than along be and ec, and we may thus replace the line segment L_2 with be and ec. This yields a faster path containing only two line segments: ae and ed.

Similarly, if $\beta \geq 1$, we may replace the portion of the original path given by $L_1 + L_2 + cg$ with ag. Indeed, in this case $\tau(af) \leq \tau(ab) + \tau(bf)$, $\tau(bc) = \tau(fg)$, which means that the resulting path is at least as fast as the original but contains only two line segments: ag and gd.

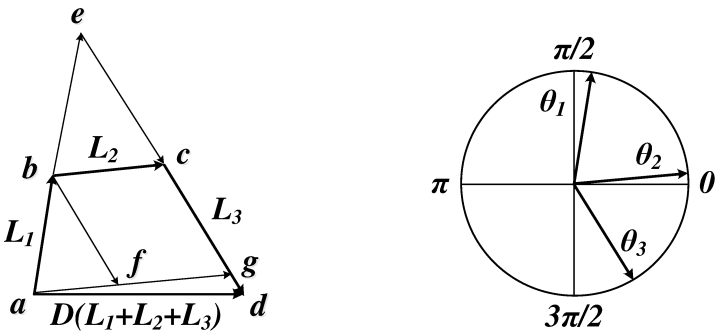

Figure 17: Total displacement achieved by the three straight line segments L_1, L_2 and L_3 and their respective headings θ_1, θ_2 and θ_3 represented on a trigonometric circle in the case where $\|\Theta_R(\theta_1, \theta_3)\| < \pi$.

(ii) $\|\Theta_R(\theta_1, \theta_3)\| \geq \pi$**:** See Figure 18. We let g be the intersection of L_3 and the line passing through a and parallel to L_2. In this case we can readily replace the portion of the original path given by $L_1 + L_2 + cg$ by ag. Since ag is shorter than L_2 and gd is shorter than L_3, it appears that the new path is faster than the original while containing only two straight line segments: ag and gd.

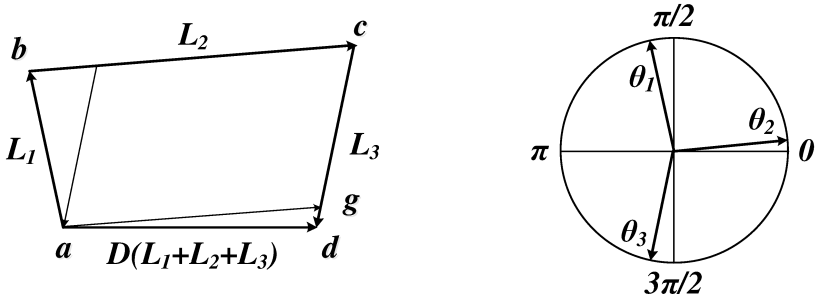

Figure 18: Total displacement achieved by the three straight line segments L_1,L_2 and L_3 and their respective headings θ_1, θ_2 and θ_3 represented on a trigonometric circle in the case where $\|\Theta_R(\theta_1, \theta_3)\| \geq \pi$.

□

We now know that there exists an optimal path that contains at most two line segments. However, at this point we know little about the number and properties of the curves and turns in the *relaxed-optimal sub-path*. The next propositions establish results that help us further narrow the characteristics of the optimal path.

Proposition 19. *There exists a fastest* relaxed-feasible sub-path *that does not contain any curves spanning the heading angles belonging to the* interior *of* $\Theta_R(\theta_s, \theta_t)$. *In other words, we can construct a* relaxed-optimal sub-path *such that it does not contain any curves* $\mathcal{C}_k(\theta_1, \theta_2)$ *for* $k \in \{R, L\}$ *if* $\Theta_k(\theta_1, \theta_2) \bigcap (\Theta_R(\theta_s, \theta_t)/\{\theta_s, \theta_t\}) \neq \emptyset$.

Before giving a proof, we present an intuitive discussion of the proposition. Proposition 19 states that making turns spanning headings already spanned by the necessary turn is redundant and, as we show in the proof, those turns could be replaced by a straight line segment yielding a path at least as fast. More generally, the idea is that turns are less 'efficient' in covering distance towards the destination than straight line segments. In any sharpest turn curve, we can find a heading whose speed towards the destination is at least as good as the speed of the other headings spanned during that turn and we would be better off following a straight line with that particular heading. We thus see turns as a necessary cost towards reaching the more favorable headings, and because of that we would only want to span headings that are not already spanned by the necessary turn $\mathcal{C}_R(\theta_s, \theta_t)$ in order to reach those headings. There is then, as we discussed in the beginning of Section 3.3, a trade-off to be made between that cost and the gain obtained by using the favorable headings.

Recall from the beginning of Scenario II that the total heading change of a *relaxed-feasible sub-path* has to be 0 mod 2π. We are currently considering Scenario II (b), and the assumption that there is no 2π-curve in the *relaxed-feasible sub-path* enables us to state a stronger property: any curve realized in the sub-path must be accompanied by its reverse equivalent. More precisely, if the sub-path contains a curve $\mathcal{C}_R(\theta_1, \theta_2)$ (respectively $\mathcal{C}_L(\theta_1, \theta_2)$), then it must also contain a curve $\mathcal{C}_L(\theta_2, \theta_1)$ (respectively $\mathcal{C}_R(\theta_2, \theta_1)$). We use this property in the proof of Proposition 19 hereunder.

Proof of Proposition 19. Suppose the sub-path contains a curve $\mathcal{C}_k(\theta_1, \theta_2)$ for $k \in \{R, L\}$ such that $\Theta_k(\theta_1, \theta_2) \bigcap (\Theta_R(\theta_s, \theta_t)/\{\theta_s, \theta_t\}) \neq \emptyset$. We have already stated that the *relaxed-feasible sub-path* must also necessarily contain the reverse curve $\mathcal{C}_{k'}(\theta_2, \theta_1)$ where $k' = \{R, L\} \setminus \{k\}$ in order for the total angular change of the sub-path to be null. Without loss of generality, we may thus assume that the sub-path contains the turns $\mathcal{C}_R(\theta_1, \theta_2)$ and $\mathcal{C}_L(\theta_2, \theta_1)$.

There then exists a set of angles that is spanned at least three times in the course of the path, once during the necessary turn $\mathcal{C}_R(\theta_s, \theta_t)$, once during $\mathcal{C}_R(\theta_1, \theta_2)$ and once during $\mathcal{C}_L(\theta_2, \theta_1)$. Let $\Theta_R(\theta_i, \theta_f) := \Theta_R(\theta_1, \theta_2) \bigcap (\Theta_R(\theta_s, \theta_t)/\{\theta_s, \theta_t\})$ be the set of such headings (for example $(\theta_i, \theta_f) = (\theta_s, \theta_2)$ in Figure 19), and consider the total displacement associated with the curves $\mathcal{C}_R(\theta_i, \theta_f) + \mathcal{C}_L(\theta_f, \theta_i)$, which are part of the sub-path. Let θ_D correspond to the heading of that displacement. Without loss of generality, we may assume that $||\Theta_k(\theta_i, \theta_f)|| \leq \pi$ for $k \in \{R, L\}$ (since the curve can otherwise be split into pieces that satisfy this assumption), in which case we know that $\theta_D \in \Theta_R(\theta_i, \theta_f)$ (Property 8).

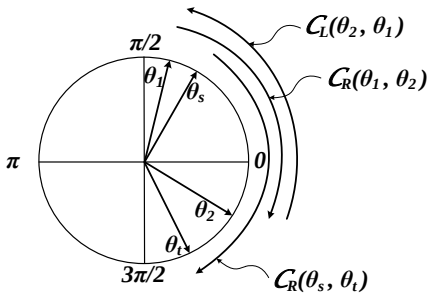

Figure 19: Heading angle representation of the sub-path curves intersecting the necessary turn headings on a trigonometric circle.

Furthermore, there exist $\tilde{\theta}_d, \tilde{\theta}_u \in \Theta_R(\theta_i, \theta_f)$ such that the path consisting of two line segments with headings $\tilde{\theta}_d$ and $\tilde{\theta}_u$ realizes the same total displacement as the two initial curves and is at least as fast as the latter. This is because by considering only the two curves $\mathcal{C}_R(\theta_1, \theta_2) + \mathcal{C}_L(\theta_2, \theta_1)$, we may restrict ourselves to the speed polar plot $\tilde{V}(\theta)$ defined by $\tilde{V}(\theta) = V(\theta)$, if $\theta \in \Theta_R(\theta_i, \theta_f)$, and $\tilde{V}(\theta) = 0$, otherwise. Since the heading of the displacement achieved by the two curves also lies in

$\Theta_R(\theta_i, \theta_f)$, we can apply Property 5 to find two such headings $\tilde{\theta}_d, \tilde{\theta}_u \in \Theta_R(\theta_i, \theta_f)$. Consequently, we replace the curves $\mathcal{C}_R(\theta_i, \theta_f) + \mathcal{C}_L(\theta_f, \theta_i)$ with these two line segments, which yields a (still *relaxed-feasible*) path that is at least as fast and does not contain any curve $\mathcal{C}_k(\theta_1, \theta_2)$ for $k \in \{R, L\}$ such that $\Theta_k(\theta_1, \theta_2) \bigcap (\Theta_R(\theta_s, \theta_t)/\{\theta_s, \theta_t\}) \neq \emptyset$ (see Figure 20). Note that this new path maintains *relaxed-feasibility* property (i.e., it is a *feasible transformation*) because the headings of the newly inserted lines belong to the set of headings already spanned by the necessary turn $\mathcal{C}_R(\theta_s, \theta_t)$.

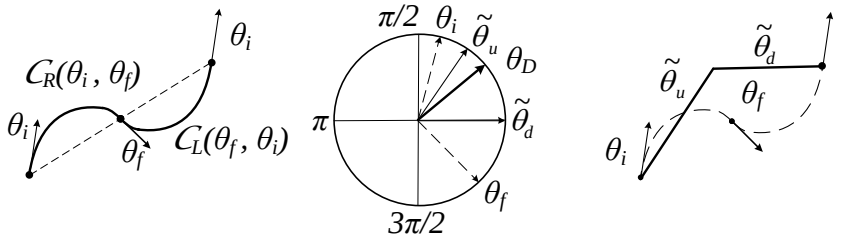

Figure 20: Replacing curves with overlapping angles by two straight lines.

□

Proposition 20. *There exists a* relaxed-optimal sub-path *such that the only curves it can contain are* $\mathcal{C}_L(\theta_s, \theta_s^*)$ *(accompanied by* $\mathcal{C}_R(\theta_s^*, \theta_s)$*) and* $\mathcal{C}_R(\theta_t, \theta_t^*)$ *(accompanied by* $\mathcal{C}_L(\theta_t^*, \theta_t)$*), for some* $\theta_s^*, \theta_t^* \in S^1$ *such that* $\Theta_L(\theta_s, \theta_s^*) \bigcap \Theta_R(\theta_t, \theta_t^*) = \emptyset$.

Proof. Proposition 19 tells us that there exists a *relaxed-optimal sub-path* such that none of its curves span the interior of the set $\Theta_R(\theta_s, \theta_t)$. At the same time, the minimum turning radius constraint implies that there cannot be any discontinuity in the interval of heading angles spanned by the complete path. Consequently, the curve segments must start (and end, when followed by the corresponding time reversed curve) with the heading angles either equal to θ_s or θ_t. Proposition 19 also implies that a curve starting with heading θ_s cannot be a right-hand turn curve, and a curve starting with θ_t cannot be a left-hand turn curve. Finally, the set of headings spanned by the two pairs of curves cannot intersect, otherwise the intersection can be replaced by two straight lines similar to the proof of Proposition 19. The same proposition implies that there would not be any additional curves spanning the angles belonging to set $\Theta_R(\theta_s^*, \theta_t^*)$. Consequently, we are left as only possible curves the couples $\{\mathcal{C}_L(\theta_s, \theta_s^*), \mathcal{C}_R(\theta_s^*, \theta_s)\}$ and $\{\mathcal{C}_R(\theta_t, \theta_t^*), \mathcal{C}_L(\theta_t^*, \theta_t)\}$ where θ_s^* and $\theta_t^* \in S^1$ are such that $\Theta_L(\theta_s, \theta_s^*) \bigcap \Theta_R(\theta_t, \theta_t^*) = \emptyset$. □

Observation 21. *A direct consequence of Proposition 20 is that the concatenation of the curve segments of an optimal path for Scenario II (b) cannot exceed three turns given by* $\mathcal{C}_L(\theta_s, \theta_s^*), \mathcal{C}_R(\theta_s^*, \theta_t^*)$ *and* $\mathcal{C}_L(\theta_t^*, \theta_t)$.

We also know from Proposition 18 that there exists an optimal path with at most two line segments. However, we do not yet know how those line segments are inserted in the curves. Combining these two results yields that the structure of an optimal path derived so far can be of several forms depending on where the straight line segments appear in the path. If they were to be inserted only between curves of different turning directions, the structure would be simply $\mathcal{CSCSC}$, where $\mathcal{C}$ designates a sharpest turn (either left-hand $\mathcal{L}$ or right-hand $\mathcal{R}$) and $\mathcal{S}$ a straight line segment. If, on the other hand, we allowed them to be inserted at any place in a curve, the structure that an optimal path could take would be more diverse. More specifically the list of all possible paths is:

1. $\mathcal{CSCSC}$ and its degenerate forms;
2. $\mathcal{CCSCSCC}$;
3. $\mathcal{CCSCSC}$ and its reversed equivalent $\mathcal{CSCSCC}$;
4. $\mathcal{CCCSCSC}$ and its reversed equivalent $\mathcal{CSCSCCC}$;

5. $\mathcal{CSCCSC}$;

6. $\mathcal{CCSCCSC}$ and its reversed equivalent $\mathcal{CSCCSCC}$;

7. $\mathcal{CSCCCSC}$.

Recall that in the listed possible paths, the concatenation of the curve segments does not exceed three turns, equivalently there are no more than two changes in turning direction along the path. Also note that in our notation, two consecutive $\mathcal{C}$ imply a change of turning direction. Our next objective is to show that the structure of an optimal path actually takes the first form $\mathcal{CSCSC}$. In other words, we prove the intuitive idea that the curves 'take us' to the desired headings of the straight line segments and that we want to limit turning along the curves as much as possible. We establish this result by progressively eliminating some of the candidate paths in order to eventually leave only the first candidate and showing that the latter cannot be reduced further.

The next proposition states that the cases 5, 6 and 7 can be reduced to one of the cases 1, 2, 3 or 4.

Proposition 22. *There exists an optimal path such that it does not contain more than one curve in between two straight lines. That is, there are no curves with opposite turning directions between the line segments.*

Proof. The proof of this proposition makes use of Property 14 which lets us rearrange segments of a path any way we wish as long as we maintain feasibility. Suppose an optimal path is such that it contains at least two curves with opposite turning directions in between two straight line segments L_1 and L_2 with respective headings θ_1 and θ_2. Such path has a structure of type 5, 6 or 7. We here show the proof for a path of type 7, the argument being almost identical for a path of type 5 or 6, and therefore omitted.

In order to satisfy Propositions 19 and 20, the only possible combination that allows at least two curves in between the straight line segments in a path of type 7 is: $C_L(\theta_s, \theta_1)L_1\mathcal{C}_L(\theta_1, \theta_s^*)\mathcal{C}_R(\theta_s^*, \theta_t^*)\mathcal{C}_L(\theta_t^*, \theta_2)L_2$ $\mathcal{C}_L(\theta_2, \theta_t)$. Using property 14 we may rearrange the segments so that the path contains only one curve between L_1 and L_2. We do this by considering instead the path $C_L(\theta_s, \theta_s^*)\mathcal{C}_R(\theta_s^*, \theta_1)L_1\mathcal{C}_R(\theta_1, \theta_2)L_2\mathcal{C}_R(\theta_2, \theta_t^*)$ $\mathcal{C}_L(\theta_t^*, \theta_t)$. In such manner, we can produce a feasible path with the same travel time satisfying the statement of the proposition. □

The next step is to show that an optimal path of type 4 (i.e., $\mathcal{CCCSCSC}$) can be reduced to a path of type 2.

Proposition 23. *Any optimal path of the type $\mathcal{CCCSCSC}$ (or its reversed equivalent $\mathcal{CSCSCCC}$) can be transformed into a path of the type $\mathcal{CCSCSCC}$, with the same travel time.*

Proof. Suppose an optimal path has the form $\mathcal{CCCSCSC}$. It can thus be written as $\mathcal{C}_L(\theta_s, \theta_s^*)\mathcal{C}_R(\theta_s^*, \theta_t^*)$ $\mathcal{C}_L(\theta_t^*, \theta_1)L_1\mathcal{C}_L(\theta_1, \theta_2)L_2\mathcal{C}_L(\theta_2, \theta_t)$. Property 14 lets us rearrange the segments as $\mathcal{C}_L(\theta_s, \theta_s^*)\mathcal{C}_R(\theta_s^*, \theta_2)$ $L_2\mathcal{C}_R(\theta_2, \theta_1)L_1\mathcal{C}_L(\theta_1, \theta_t^*)\mathcal{C}_L(\theta_t^*, \theta_t)$. The same argument applies to $\mathcal{CSCSCCC}$. □

Propositions 22 and 23 enable us to narrow down the list of possible optimal paths to only the first three types of paths.

The next proposition demonstrates that there exists an optimal path which does not contain a structure of the form $\mathcal{CCSCSC}$ or $\mathcal{CSCSCC}$. This will eliminate the paths of types 2 and 3 and will let us conclude that in the case of Scenario II (b), there exists an optimal path of the type 1, that is $\mathcal{CSCSC}$.

Proposition 24. *In the case where $\nexists(\theta_u, \theta_d) \in \mathcal{U}(R,t) \times \mathcal{D}(R,t)$ such that $(\theta_u, \theta_d) \in \Theta_R(\theta_s, \theta_t)$ and a sub-path does not contain a 2π-curve, there exists an optimal path which does not contain a segment of the form $\mathcal{CCSCSC}$ or $\mathcal{CSCSCC}$ (where the straight line segments are not null).*

The idea behind Proposition 24 is that when a path begins (respectively ends) with two curves and already includes two straight line segments, it contains a superfluous portion. We show that such a path is either not optimal, or can be *feasibly transformed* into a path of the from $\mathcal{CSCSC}$.

Proof. See Appendix A.1 □

Proposition 24 now lets us assert that in Scenario II (b), there exists an optimal path of the form $\mathcal{CSCSC}$, along with its possible degenerate cases.

3.3.4 Characterization of an optimal path

We have just shown that in the case of Scenario II (b), there exists an optimal path of the form $\mathcal{CSCSC}$. This result actually extends to the other scenarios as we state in the next theorem which represents our key result.

Theorem 25. *There exists an optimal path from an initial configuration (x_s, y_s, θ_s) to a target configuration (x_s, y_s, θ_s) such that it is a portion of a path of type $\mathcal{CSCSC}$ where $\mathcal{C}$ denotes a sharpest turn and $\mathcal{S}$ a straight line.*

Proof. We first show that for each of the scenarios discussed above, we can write the form of an optimal path as $\mathcal{CSCSC}$.

Scenario I: In Scenario I, Proposition 16 showed that we could insert the two straight lines directly into the necessary turn $\mathcal{C}_R(\theta_s, \theta_t)$. Consequently, we may write an optimal path as $\mathcal{C}_R(\theta_s, \theta_1)\mathcal{SC}_R(\theta_1, \theta_2)\mathcal{SC}_R(\theta_2, \theta_t)$.

Scenario II (a): Scenario II (a) contains the necessary turn $\mathcal{C}_R(\theta_s, \theta_t)$ and a 2π-turn which we choose to be $\mathcal{C}_{R,2\pi}(\theta_t)$ without violating the feasibility of the path. From Property 14, an optimal path can then take the form $\mathcal{C}_R(\theta_s, \theta_t)\mathcal{C}_R(\theta_t, \theta_1)\mathcal{SC}_R(\theta_1, \theta_2)\mathcal{SC}_R(\theta_2, \theta_t)$ where we have explicitely divided the first turn into two to highlight the fact that the turn spans potentially more than 2π. The structure of the optimal path is still however of the form $\mathcal{CSCSC}$.

Scenario II (b): We already stated in the conclusion of Proposition 24 that in Scenario II (b) there existed an optimal path of the form $\mathcal{CSCSC}$.

We have however only derived necessary conditions in order not to violate optimality, which does not guarantee that such formula is the shortest possible one. In order to prove that the structure of the optimal paths cannot be reduced any further, we need to exhibit one example for which we know that a path with structure $\mathcal{CSCSC}$ is indeed optimal. Such example is constructed as follows. Consider an initial point with coordinates (x_s, y_s) and assume the speed polar plot is as presented in Figure 21. We choose θ_s and θ_t such that there exists a heading belonging to $\Theta_R(\theta_s, \theta_t)$ for which we can find its corresponding θ_u and θ_d in the angles span by $\mathcal{C}_R(\theta_s, \theta_t)$ (assuming $\mathcal{C}_R(\theta_s, \theta_t)$ is faster than $\mathcal{C}_L(\theta_s, \theta_t)$).

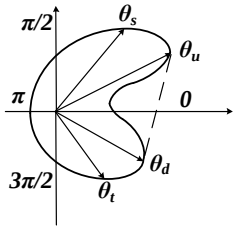

Figure 21: Speed polar plot used to construct an optimal path of the form $\mathcal{CSCSC}$.

We then place the final point on the line starting from (x_R, y_R) with that heading (see Figure 22). We know that the fastest path from (x_R, y_R) to (x_t, y_t) is found by using straight lines with headings θ_u and θ_d. Those straight line segments can be inserted in the necessary turn $\mathcal{C}_R(\theta_s, \theta_t)$, which consequently yields a fastest path from (x_s, y_s) to (x_t, y_t). This path being of the form $\mathcal{CSCSC}$, it proves our claim. □

Theorem 25 presents one of the key results of this paper by characterizing the structure of an optimal path between any given initial and final configurations. So far, we have considered the fastest-path finding problem for general direction-dependent speed and minimum turning radius functions; and this general structure of the problem prevents us from further characterizing an optimal path and delivering an implementable algorithm. An optimal path for a vehicle is highly dependent on the characteristics of its speed polar plot and the shapes of the sharpest-turn curves and can only be further analyzed on a case-by-case bases. In the following Section 3.4, we make a specific assumption on the agents

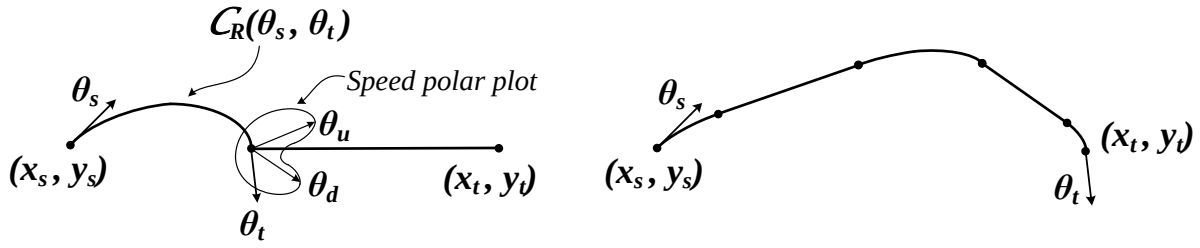

Figure 22: Example yielding an optimal path of the form $\mathcal{CSCSC}$.

speed function and deliver an algorithm that constructs an optimal path in the case of a *convex* speed polar plots. This special case includes the Dubins car problem and path finding in the presence of constant and uniform flow (e.g., wind or current), while encompassing a broader set of problems. We also demonstrate an application of our results to a non-convex speed polar plot of the vessel routing problem that motivated our research (Section 4), and Appendix B outlines the supporting calculations that illustrate the application of Theorem 25 to a real-life problem. The development of a tractable algorithm synthesizing the optimal path structure for more general problem instances is part of our future work.

3.4 Structure of an Optimal Path for a Convex Speed Polar Plot

In the preceding sections we have analyzed a general problem by making only minimal assumptions on the properties of the speed function, namely that it is C^∞ and greater than zero. In this section we look at a special case of our problem where the speed polar plot is convex. Dubins car problem is a particular case of the convex case, but remain more general than Dubins' since we do not restrict to a constant speed and constant turning radius.

First, we establish the key property of the convex case, which does not hold true for more general non-convex case. The main distinction comes in the stronger form of Property 5 which we state in the following Lemma.

Lemma 26 (adapted from (Dolinskaya & Smith, 2012))**.** *In the case of a convex speed polar plot, the travel time along the straight line path from $a \in \mathbb{R}^2$ to $b \in \mathbb{R}^2$ is never greater than that of any other path from a to b.*

To incorporate bounded curvature, we establish a more general result in the following theorem.

Theorem 27. *Consider a rectifiable (i.e., finite-length) path p^* from point $a \in \mathbb{R}^2$ to point $b \in \mathbb{R}^2$ such that the curve p^* and a line segment ab enclose a convex set $S_{p^*} \subseteq \mathbb{R}^2$ (i.e., a* convex path*). Consider another path p from a to b, and let $S_p \subseteq \mathbb{R}^2$ denote the set of points enclosed by the curve p and a line segment ab. Then, when the movement along a path is characterized by a speed function with a convex polar plot, the travel time along path p^* is never greater than the travel time along path p if $S_{p^*} \subseteq S_p$ (see Figure 23).*

Proof. See Appendix A.2. □

Recall from Property 5 that the fastest path between two points for the case of a non-convex speed polar plot can be obtained by following *two* straight line segments when the minimum turning radius constraint is ignored. In the convex speed polar plot case, *one* straight line segment satisfies this property. Thus, by following discussion analogous to Section 3.3, while employing Lemma 26 instead of Property 5, we can reduce the number of straight line segments in the optimal path structure from two to one and more precisely characterize an optimal path.

Below, we follow the same steps as for the non-convex case and adapt the results when possible, keeping the same notations as in Section 3.3.

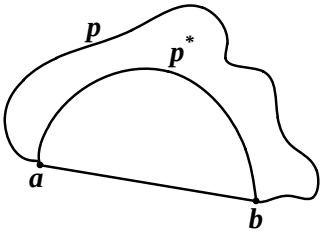

Figure 23: Example of paths p^* and p as described in Theorem 27.

3.4.1 Lower and upper bounds on minimum travel time from (x_s, y_s, θ_s) to (x_t, y_t, θ_t) in the convex case

The new bounds on minimal travel time are readily re-derived following the same logic as in Section 3.3.2 while using Lemma 26 instead of Property 5. We then obtain:

$$LB_R = \tau(\mathcal{C}_R(\theta_s, \theta_t)) + \tau(D_{Rt}), \tag{27}$$
$$LB_L = \tau(\mathcal{C}_L(\theta_s, \theta_t)) + \tau(D_{Lt}), \tag{28}$$
$$LB = \min\{LB_R; LB_L\}. \tag{29}$$

Similarly, we obtain the upper bound as:

$$UB_R = \tau(\mathcal{C}_R(\theta_s, \theta_t)) + \tau(\mathcal{C}_{2\pi}) + \tau(D_{Rt} - D(\mathcal{C}_{2\pi})), \tag{30}$$
$$UB_L = \tau(\mathcal{C}_L(\theta_s, \theta_t)) + \tau(\mathcal{C}_{2\pi}) + \tau(D_{Lt} - D(\mathcal{C}_{2\pi})), \tag{31}$$
$$LB = \min\{UB_R; UB_L\}. \tag{32}$$

3.4.2 Characterization of a *relaxed-optimal sub-path* in the convex case

Analogous to Section 3.3.3, we break the analysis of a *relaxed-optimal sub-path* starting at (x_R, y_R) in two main scenarios. However, the differentiating factor here is whether $\alpha(D_{Rt}) \in \Theta_R(\theta_s, \theta_t)$ since the fastest path from (x_R, y_R) to (x_s, y_s) can be obtained by the straight line segment joining (x_R, y_R) to (x_s, y_s).

Scenario I: $\alpha(D_{Rt}) \in \Theta_R(\theta_s, \theta_t)$.

Proposition 28. *The straight line segment from (x_R, y_R) to (x_t, y_t) is a fastest* relaxed-feasible sub-path*, if the slope of the displacement vector from (x_R, y_R) to (x_t, y_t), i.e., D_{Rt}, is equal to one of the heading angles spanned by the right-hand sharpest turn curve $\mathcal{C}_R(\theta_s, \theta_t)$.*
That is, if $\alpha(D_{Rt}) \in \Theta_R(\theta_s, \theta_t)$ then a fastest path from (x_s, y_s) to (x_t, y_t) containing segments making up a right-hand sharpest turn curve is equal to the curve $\mathcal{C}_R(\theta_s, \alpha(D_{Rt}))$, followed by a straight line segment D_{Rt} and finally followed by the curve $\mathcal{C}_R(\alpha(D_{Rt}), \theta_t)$, see Figure 24.

Proof. If $\alpha(D_{Rt}) \in \Theta_R(\theta_s, \theta_t)$, the straight line segment D_{Rt} is a *relaxed-feasible sub-path*, and LB_R and equation (27) imply it is a *relaxed-optimal sub-path*. □

Scenario II: $\alpha(D_{Rt}) \notin \Theta_R(\theta_s, \theta_t)$. Recall that the necessary heading change from θ_s to θ_t is already accomplished by the curve $\mathcal{C}_R(\theta_s, \theta_t)$ outside of the sub-path, and the cumulative heading change along any *relaxed-feasible sub-path* must be equal to zero or 2π.

Scenario II(a): $\alpha(D_{Rt}) \notin \Theta_R(\theta_s, \theta_t)$ and sub-path contains a 2π curve.

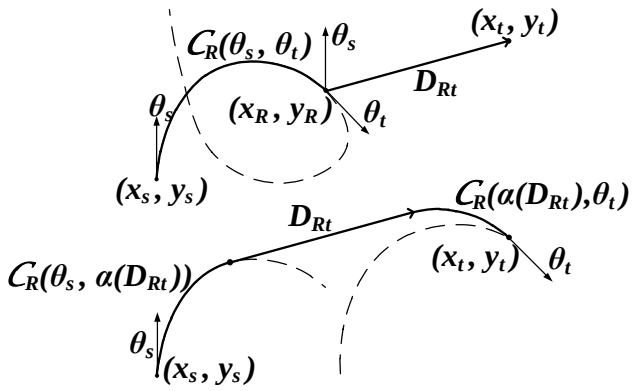

Figure 24: Construction of an optimal path as described in Proposition 28.

Proposition 29. *If a* relaxed-optimal sub-path *contains a* 2π*-curve, a fastest* relaxed-feasible sub-path *consists of a curve* $\mathcal{C}_{R,2\pi}(.)$ *or* $\mathcal{C}_{L,2\pi}(.)$ *and a straight line segment connecting point* $(x_R, y_R) + D(\mathcal{C}_{2\pi})$ *to the target point* (x_t, y_t)*.*

Proof. From the upper bound computation, in equation (30), we know that when a *relaxed-optimal sub-path* contains a 2π-curve $\mathcal{C}_{R,2\pi}(.)$ or $\mathcal{C}_{L,2\pi}(.)$, the remaining of the sub-path is a straight line. □

Scenario II(b): $\alpha(D_{Rt}) \notin \Theta_R(\theta_s, \theta_t)$ **and a sub-path does not contain a** 2π **curve.** The propositions derived in section 3.3.3 still hold, in particular Propositions 19 and 20. We now show that in the case of a convex speed polar plot, there exists an optimal path with at most one (instead of two) straight line segments.

Theorem 30. *In the case of a convex speed polar plot, there exists a* relaxed-optimal sub-path *with at most one line segment. That is, there exists a fastest* relaxed-feasible sub-path *such that it either does not contain any line segments, or all the line segments have the same heading angle and can be rearranged into a single straight line.*

Proof. See Appendix A.3. □

Proposition 31. *There exists a* relaxed-optimal sub-path *such that it can only contain the curve pairs* $\{\mathcal{C}_L(\theta_s, \theta_s^*), \mathcal{C}_R(\theta_s^*, \theta_s)\}$ *and* $\{\mathcal{C}_R(\theta_t, \theta_t^*), \mathcal{C}_L(\theta_t^*, \theta_t)\}$ *and a line segment with the slope either equal to* θ_s^* *or* θ_t^**, for some* $\theta_s^*, \theta_t^* \in S^1$ *such that* $\Theta_L(\theta_s, \theta_s^*) \bigcap \Theta_R(\theta_t, \theta_t^*) = \emptyset$*.*

Proof. See Appendix A.4. □

Proposition 32. *There exists a* relaxed-optimal sub-path *described by one of the following statements:*

1. *it consists of only two curve pairs* $\{\mathcal{C}_L(\theta_s, \theta_s^*), \mathcal{C}_R(\theta_s^*, \theta_s)\}$ *and* $\{\mathcal{C}_R(\theta_t, \theta_t^*), \mathcal{C}_L(\theta_t^*, \theta_t)\}$*, for some* $\theta_s^*, \theta_t^* \in S^1$ *such that* $\Theta_L(\theta_s, \theta_s^*) \bigcap \Theta_R(\theta_t, \theta_t^*) = \emptyset$*, or*
2. *it consists of only one curve pair either* $\{\mathcal{C}_L(\theta_s, \theta_s^*), \mathcal{C}_R(\theta_s^*, \theta_s)\}$ *or* $\{\mathcal{C}_R(\theta_t, \theta_t^*), \mathcal{C}_L(\theta_t^*, \theta_t)\}$ *for some* $\theta_s^*, \theta_t^* \in S^1$ *and a straight line segment with the slope* θ_s^* *or* θ_t^**, respectively.*

Proof. See Appendix A.5. □

3.4.3 Characterization of an optimal path for the convex case

We now combine all the cases and corresponding properties of the *relaxed-optimal sub-path* to state equivalent to the key result from Theorem 25 adapted to the convex speed polar plot case.

Theorem 33. *When the movement along a path is characterized by a speed function with a convex polar plot, an optimal path from* (x_s, y_s, θ_s) *to* (x_t, y_t, θ_t) *is of the form* $\mathcal{CCC}$*, or* $\mathcal{CSC}$*, where* $\mathcal{C}$ *denotes a sharpest turn curve and* S *denotes a straight line segment. It is implied that a path of the form* $\mathcal{CCC}$ *alternatively switches between left-hand and right-hand sharpest turn curves.*

Proof. The preceding propositions list all the possible forms of the optimal path candidates; we show that each is either of the form $\mathcal{CCC}$ or $\mathcal{CSC}$. We discuss the case when an optimal path has to contain the curve $\mathcal{C}_R(\theta_s, \theta_t)$; the case when an optimal path has to contain the curve $\mathcal{C}_L(\theta_s, \theta_t)$ is analogous.

Scenario I: A *relaxed-optimal sub-path* is a straight line equal to D_{Rt} (Proposition 28).
A path consisting of the curve $\mathcal{C}_R(\theta_s, \alpha(D_{Rt}))$ followed by a straight line segment D_{Rt} which is followed by the curve $\mathcal{C}_R(\alpha(D_{Rt}), \theta_t)$ is of the form $\mathcal{CSC}$.

Scenario II(a): A fastest *relaxed-feasible sub-path* consists of a 2π-curve and a straight line segment from the point $(x_R, y_R) + D(\mathcal{C}_{2\pi})$ to the target point (x_t, y_t) (Proposition 29).
Let D_1 denote a displacement vector from point $(x_R, y_R) + D(\mathcal{C}_{2\pi})$ to the target point (x_t, y_t). Then an optimal path is as follows: a curve $\mathcal{C}_R(\theta_s, \theta_t)\mathcal{C}_R(\theta_t, \alpha(D_1))$, followed by a line segment equal to D_1, and concluded with a curve $\mathcal{C}_R(\alpha(D_1), \theta_t)$, which is of the form $\mathcal{CSC}$.

Scenario II(b) case 1: A *relaxed-optimal sub-path* consists of only curves $\mathcal{C}_L(\theta_s, \theta_s^*)$ (accompanied by $\mathcal{C}_R(\theta_s^*, \theta_s)$) and $\mathcal{C}_R(\theta_t, \theta_t^*)$ (accompanied by $\mathcal{C}_L(\theta_t^*, \theta_t)$) (Proposition 32).
An optimal path is as follows (in order to maintain the heading continuity): a curve $\mathcal{C}_L(\theta_s, \theta_s^*)$, followed by a curve $\mathcal{C}_R(\theta_s^*, \theta_t^*) = \mathcal{C}_R(\theta_s^*, \theta_s)\mathcal{C}_R(\theta_s, \theta_t)\mathcal{C}_R(\theta_t, \theta_t^*)$ and followed by another curve $\mathcal{C}_L(\theta_t^*, \theta_t)$, which is of the form $\mathcal{CCC}$.

Scenario II(b) case 2: A *relaxed-optimal sub-path* consists of only one curve pair $\mathcal{C}_L(\theta_s, \theta_s^*)\mathcal{C}_R(\theta_s^*, \theta_s)$ and a straight line segment with the slope θ_s^* (Proposition 32).
Then an optimal path is a curve $\mathcal{C}_L(\theta_s, \theta_s^*)$, a straight line segment with the slope θ_s^*, and then followed by a curve $\mathcal{C}_R(\theta_s^*, \theta_t) = \mathcal{C}_R(\theta_s^*, \theta_s)\mathcal{C}_R(\theta_s, \theta_t)$. This path is of the form $\mathcal{CSC}$.

Scenario II(b) case 3: A *relaxed-optimal sub-path* consists of only one curve pair $\mathcal{C}_R(\theta_t, \theta_t^*)\mathcal{C}_L(\theta_t^*, \theta_t)$ and a straight line segment with the slope θ_t^* (Proposition 32).
Then an optimal path is a curve $\mathcal{C}_R(\theta_s, \theta_t^*) = \mathcal{C}_R(\theta_s, \theta_t)\mathcal{C}_R(\theta_t, \theta_t^*)$, a straight line segment with the slope θ_t^*, followed by a curve $\mathcal{C}_L(\theta_t^*, \theta_t)$. This path is of the form $\mathcal{CSC}$.

□

The adapted form of the key theorem of this paper, Theorem 33, explicitly characterizes an optimal path in the case of a convex speed polar plot. It is interesting to note that the structure of our optimal path is similar to that of an isotropic Dubins car problem. However, curves in our case do not generally correspond to the circle arcs as in Dubins car problem. Instead, they might have complex forms. Despite the general form of the sharpest-turn curves, we show that our problem is controllable and has an optimal solution as characterized in Theorem 33.

3.5 Optimal Path Finding Algorithm for a Convex Speed Polar Plot

We develop a path finding algorithm to facilitate the implementation of an optimal path with bounded curvature as characterized in Theorem 33. While the main premise of our algorithm is the result of Theorem 33, without explicitly knowing the values of θ_s^* and θ_t^*, the actual construction of a fastest path proves to be a challenge. Therefore, we state additional propositions in order to further characterize an optimal path depending on the target state (x_t, y_t, θ_t) relative to the initial state (x_s, y_s, θ_s).

Proposition 34. *If a* relaxed-optimal sub-path *does not contain a* 2π*-curve, there exists a* relaxed-optimal sub-path *from point* (x_R, y_R) *to point* (x_t, y_t) *such that it passes through the mid-point of the connecting line,* D_{Rt}*.*

Proof. From Proposition 31 we know that any sharpest turn curve of a *relaxed-optimal sub-path* must be accompanied by the corresponding time-reversed curve. Furthermore, Property 11 states that the displacement vector for a curve and its reversed curve are equal. Similarly, we can split a straight line segment part of a *relaxed-optimal sub-path* into two segments with equal lengths. Then, we can construct a *relaxed-optimal sub-path* such that the first and second halves of the path (in respect of time) are time-reversed of each other. We know that the total displacement vector for the first half of the path must be equal to the second half, and therefore corresponding to the vector $\frac{1}{2}D_{Rt}$. □

Any part of an optimal path has to be a minimum travel-time path, therefore we construct half of a *relaxed-optimal sub-path* with the displacement equal to $\frac{1}{2}D_{Rt}$. Then, applying Proposition 34 we set the second half of the sub-path to be the corresponding time-reversed path. Thus, Proposition 34 facilitates the construction of a *relaxed-optimal sub-path* as characterized in Theorem 33.

Before stating the proposition, we introduce notation to ensure the clarity of our arguments (see Figures 25 - 28 for examples). Let point $a = (x_R, y_R)$ and point b denote the mid-point of D_{Rt} starting at a, that is $b = a + \frac{1}{2}D_{Rt}$. Let curves $\mathcal{C}_{a,L} = \mathcal{C}_L(\theta_s, \theta_t)$ and $\mathcal{C}_{a,R} = \mathcal{C}_R(\theta_t, \theta_s)$ that start at point a and end at point $c = a + D(\mathcal{C}_{a,L}) = a + D(\mathcal{C}_{a,R})$. We let $\mathcal{S}_R \subseteq \mathbb{R}^2$ to denote a region enclosed the curve $\mathcal{C}_{a,R}$ and a line segment ac. Similarly, $\mathcal{S}_L$ is the region enclosed by $\mathcal{C}_{a,L}$ and ac. We set $\mathcal{S}' = \mathcal{S}_R \bigcup \mathcal{S}_L$.

When $\alpha(D_{Rt}) \notin \Theta_R(\theta_s, \theta_t)$ and a 2π-curve is not part of a *relaxed-optimal sub-path*, one of the following cases presented in Propositions 35 - 38 describes the half of a *relaxed-optimal sub-path*, from a to b. To prove each proposition, we demonstrate that the proposed path is faster than other candidate paths characterized in Proposition 32.

Proposition 35. *Assume that $\alpha(cb) \in \Theta_R(\theta_t, \theta_s)$ and $b \notin \mathcal{S}'$ (see Figure 25). There exist two lines passing through point b, such that one line is tangent to curve $\mathcal{C}_{a,L}$ and another line is tangent to curve $\mathcal{C}_{a,R}$, at the corresponding points d_L and d_R, and the slopes $\theta_{d_L} = \alpha(d_L b)$ and $\theta_{d_R} = \alpha(d_R b)$, respectively. Then, the half of a fastest* relaxed-feasible sub-path *is either the curve $\mathcal{C}_L(\theta_s, \theta_{d_L})$ followed by a line segment $d_L b$, or the curve $\mathcal{C}_R(\theta_t, \theta_{d_R})$ followed by $d_R b$.*

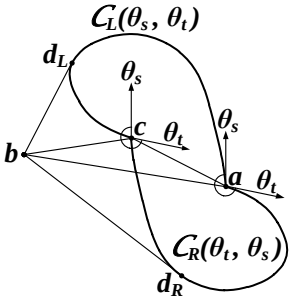

Figure 25: Illustration of Proposition 35.

Proof. When, $\alpha(cb) \in \Theta_R(\theta_t, \theta_s)$ and $b \notin \mathcal{S}'$, the constructed straight line segments $d_R b$ and $d_L b$ are faster than part of a second sharpest turn curve ending at point b (Theorem 27), since the second curves ending at point b either would not intersect the curves starting at point a or the set of heading angles spanned by parts of the two curves would overlap. □

Proposition 36. *Assume that $\alpha(cb) \notin \Theta_R(\theta_t, \theta_s)$ and $b \notin \mathcal{S}'$ (see Figure 26). There exists only one line passing through point b that is tangent to either curve $\mathcal{C}_{a,L}$ or $\mathcal{C}_{a,R}$ and satisfies heading angle continuity constraint. We call the tangent point d and the heading of the sharpest turn curve at that point $\theta_d = \alpha(db)$. The half of a fastest* relaxed-feasible sub-path *is the curve $\mathcal{C}.(\theta_s, \theta_d)$ followed by a line segment db.*

Proof. The constructed path is the only feasible candidate. A second curve ending at point b either would not intersect a curve starting at point a or the set of heading angles spanned by parts of the two curves would overlap. □

Proposition 37. *Assume that $\alpha(cb) \in \Theta_R(\theta_t, \theta_s)$ and $b \in \mathcal{S}'$ (see Figure 27). Due to symmetry of the argument, we assume $b \in \mathcal{S}_L$, without loss of generality. There exists a line passing through point b, tangent to curve $\mathcal{C}_{a,R}$, at point d with the heading of the sharpest turn curve at that point $\theta_d = \alpha(db)$. In addition, a curve $\mathcal{C}_L(\theta_s, \theta_t)$ ending at point b, denoted by $\mathcal{C}_{b,L}(\theta_s, \theta_t)$, intersects the curve $\mathcal{C}_{a,L} = \mathcal{C}_L(\theta_s, \theta_t)$ at some point denoted by e. Then, the half of a fastest* relaxed-feasible sub-path *will be one of the two paths: (1) curve $\mathcal{C}_R(\theta_t, \theta_d)$ followed by a line segment db, or (2) part of the curve $\mathcal{C}_{a,L} = \mathcal{C}_L(\theta_s, \theta_t)$ between points a and e followed by part of the curve $\mathcal{C}_{b,L} = \mathcal{C}_L(\theta_s, \theta_t)$ between points e and b.*

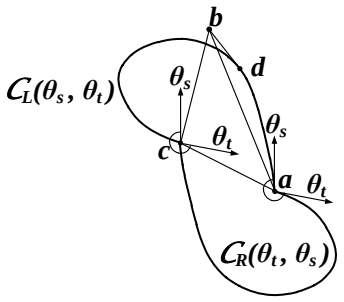

Figure 26: Illustration of Proposition 36.

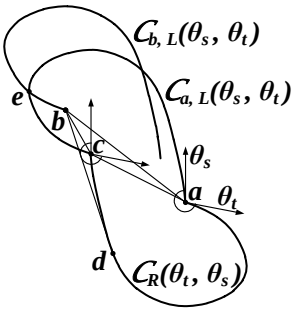

Figure 27: Illustration of Proposition 37.

Proof. For a candidate path (1), proof is analogous to Proposition 35 . For a candidate path (2), it is the only feasible candidate including a curve $\mathcal{C}_{a,L} = \mathcal{C}_L(\theta_s, \theta_t)$. □

Proposition 38. *Assume that $\alpha(cb) \notin \Theta_R(\theta_t, \theta_s)$ and $b \in \mathcal{S}'$ (see Figure 28). Due to symmetry of the argument, we assume $b \in \mathcal{S}_L$, without loss of generality. Then, a curve $\mathcal{C}_L(\theta_s, \theta_t)$ ending at point b, denoted by $\mathcal{C}_{b,L}(\theta_s, \theta_t)$, intersects the curve $\mathcal{C}_{a,L} = \mathcal{C}_L(\theta_s, \theta_t)$ at a point denoted by e. And, the half of a fastest* relaxed-feasible sub-path *is part of the curve $\mathcal{C}_{a,L} = \mathcal{C}_L(\theta_s, \theta_t)$ between points a and e followed by part of the curve $\mathcal{C}_{b,L} = \mathcal{C}_L(\theta_s, \theta_t)$ between points e and b.*

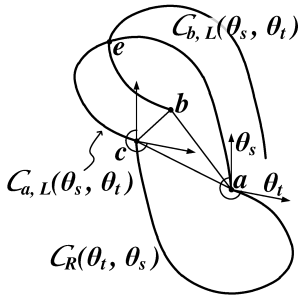

Figure 28: Illustration of Proposition 38.

Proof. The constructed path is the only feasible candidate. A second curve ending at point b either would not intersect a curve starting at point a or the set of heading angles spanned by parts of the two curves would overlap. □

We would like to note that in order to ensure that our analysis and results can be implemented to a wide variety of applications, we make no specific restrictions on the minimum turning radius function. However, this general direction-dependent function produces a diverse set of sharpest turn curves and limits how specific and definitive our path characteristic can be. Therefore, despite similar characterizations, the construction of an optimal path for our problem is more evolved than for Dubins car problem.

We now present Algorithm 1 which finds a fastest path with bounded curvature for a direction-dependent speed function corresponding to a convex speed polar plot. We know that an optimal path has to contain a curve $\mathcal{C}_R(\theta_s, \theta_t)$ or $\mathcal{C}_L(\theta_s, \theta_t)$, and without knowing more specific information about the functions $R(\theta)$ and $V(\theta)$ we cannot conclude which one of these cases is optimal. Consequently, we construct paths for each scenario and compare their corresponding minimum travel times.

Algorithm 1 Fastest Path with Bounded Curvature for a Convex Speed Polar Plot.

Step 1. For each cases, $k = R$ and $k = L$:

Step 1a. Set $\tau_k = \infty$.

Step 1b. Set $a = (x_s, y_s) + D(\mathcal{C}_k(\theta_s, \theta_t))$ and $D_{at} = (x_t, y_t) - a$.
If $\alpha(D_{at}) \in \Theta_k(\theta_s, \theta_t)$, compute the travel time $\tau_k = \tau(\mathcal{C}_k(\theta_s, \theta_t)) + \tau(D_{at})$. Skip steps 1c and 1d for current k value.

Step 1c. Set $a' = a + D(\mathcal{C}_{2\pi})$ and $D_{a't} = (x_t, y_t) - a'$.
$\tau_k = \min\{\tau_k, \tau(\mathcal{C}_k(\theta_s, \theta_t)) + \tau(\mathcal{C}_{2\pi}) + \tau(D_{a't})\}$.

Step 1d. Set $b = a + \frac{1}{2} D_{at}$. Construct an optimal sub-path as described in Propositions 35 - 38 and update τ_k if the found path is faster.

Step 2. Compare τ_R and τ_L; the smaller value is the minimum travel time, and a path corresponding to that travel time is optimal.

4 Application: Vessel Routing in a Stationary Random Seaway

In this section, we present an application of our results to a short-range vessel routing problem in a stationary random seaway that motivated our work. Figure 1 in Section 1 illustrates a speed polar plot of the S175 containership used as a test vessel for our numerical results. We apply our results for the non-convex speed polar plot (Theorem 25) to characterize the structure on an optimal path for various scenarios of the problem instance and quantify the decrease in travel time along the found paths, as opposed to following the paths suggested by the preceding literature (Dubins car path and paths found for direction-dependent convex speed polar plots, e.g., in the presence of constant flow vector). We also present an example of the optimal path synthesis for our problem. (More comprehensive path synthesis for generalized sets of problems is part of our future work.) Appendix B contains the supporting calculations for our numerical results.

Consider the speed polar plot of the S175 containership introduced in Section 1 (Figure 1), which we plot in a Cartesian coordinate system in Figure 29. Note that the speed interpolations for the two figures differ slightly, however this does not impact the validity of our results (the precise interpolation of the speed plot would involve fitting sophisticated physical models, which is outside the scope of this paper). The containership motions are subject to a minimum-turning radius constraint, which is a function of its direction-dependent speed and, consequently, is a function of the vessel's heading direction. Figure 30 plots the minimum-turning radius values versus the containership's speed and its heading angle.

We examine a particular instance of our problem in order to demonstrate the properties and results derived in this paper, as well as, highlight the effects of the non-convex speed polar plot in comparison to the previous literature. Consider a coordinate system with its x-axis aligned with the 315° heading angle with respect to the dominant wave direction (*wrt dwd*), see Figure 31. Let the initial configuration be $s = (x_s, y_s) = (0, 0)$, $\theta_s = 0°$ (i.e., 315° *wrt dwd*) and the target configuration be $t = (x_t, y_t) = (L, 0)$, $\theta_t = 0°$, for some $L \geq 0$. Since $\theta_s = \theta_t = \alpha(D_{st})$, an application of the Dubins car results (as well

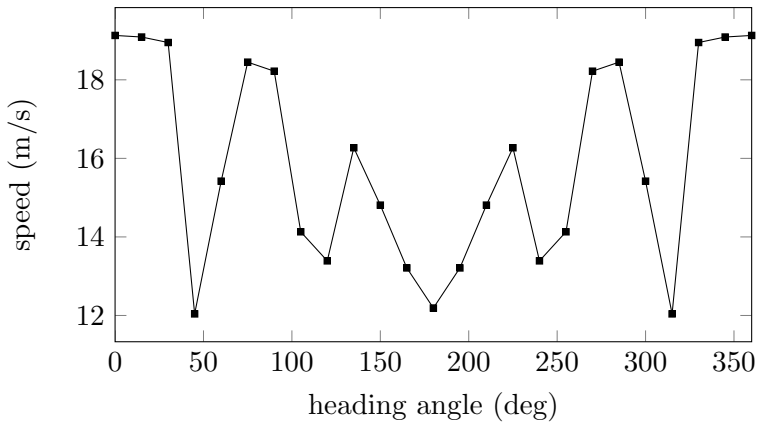

Figure 29: Speed function of the S175 containership in Sea State 7.

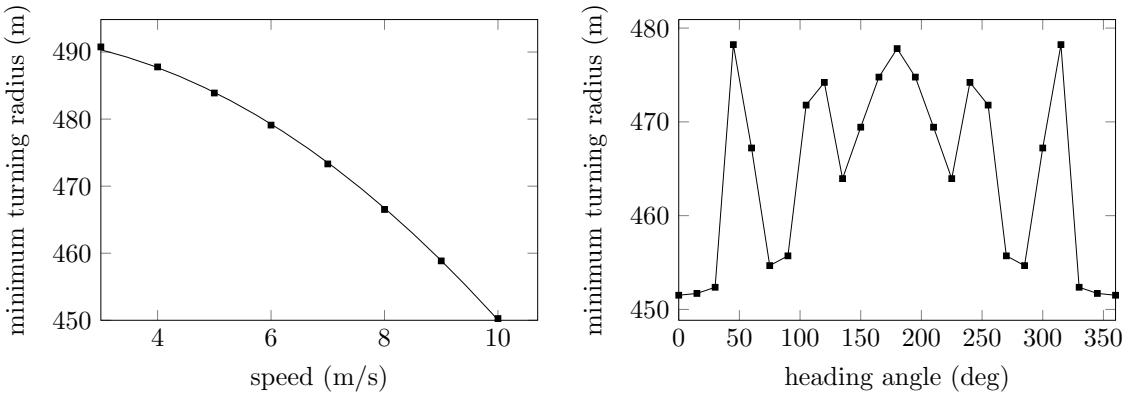

Figure 30: Minimum-turning radius of the S-175 containership plotted vs speed (left) and the heading angle relative to the dominant wave direction (right).

as results for generalized convex speed-polar plot) leads to a straight line path between the two points, D_{st}. The travel time required to cover the corresponding distance (τ_D) would thus be:

$$\tau_D(L) = \frac{L}{V(315^\circ)}. \tag{33}$$

The structure of an optimal path established in this paper is more complex than a straight line from s to t and depends on the actual value of L. From the speed polar plot, illustrated in Figure 31, we observe that the speed value increases as the vessel's heading deviates away from the initial, and final, heading within the $[285^\circ, 330^\circ]$ range *wrt dwd* (i.e., $[-30^\circ, 15^\circ]$). More importantly, the projection of the velocity on the x-axis (315° *wrt dwd*) increases and is greater than $V(315^\circ)$ within the specified range. This implies that in order to advance along the x-axis, it is beneficial to deviate from the θ_s heading angle as much as possible within this range of headings. Using the notations introduced in Section 3.1, we let $a = s$ and $b = t$, then $\theta_{ab} = 0^\circ$, $\theta^u_{ab} = 15^\circ$ and $\theta^d_{ab} = -30^\circ$. We know that in the absence of minimum turning radius constraint, the optimal path from a to b is composed of two straight line segments with headings θ^u_{ab} and θ^d_{ab} (see (Dolinskaya & Smith, 2012) for proof of these results and the discussion of how θ^u_{ab} and θ^d_{ab} are found). Consequently, for a large enough L (i.e., $L > 1,055$ meters), the agent has enough time to make the turns necessary to reach those headings, in order to capture the benefit of traveling along those two lines. Then, a fastest path from (x_s, y_s, θ_s) to (x_t, y_t, θ_t) corresponds to the $\mathcal{CSCSC}$ case and is composed of the sharpest-turn curves $\mathcal{C}_L(\theta_{ab}, \theta^u_{ab})$, $\mathcal{C}_R(\theta^u_{ab}, \theta^d_{ab})$ and $\mathcal{C}_L(\theta^d_{ab}, \theta_{ab})$, and the two straight lines S_1 and S_2 with headings θ^u_{ab} and θ^d_{ab}, respectively (Figure 32). See Appendix B

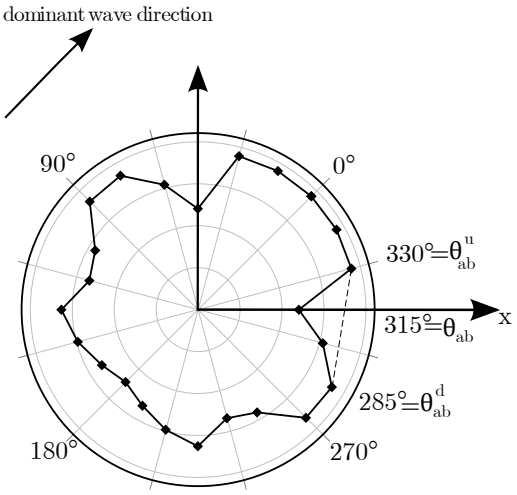

Figure 31: Speed polar plot in rotated coordinate system.

for calculation of S_1, S_2 and the values of L corresponding to this scenario.

For a relatively small values of L (i.e., $L \leq 484$ meters), the agent might not be able to make the necessary turns to reach the headings θ^u_{ab} and θ^d_{ab}, without traversing too far along the x-axis and having to make extra turns to "come back" to the point (x_t, y_t). However, it is still beneficial to deviate from the straight line path st to travel with greater speed values than $V(315°)$. Thus, an optimal path for such range of L values corresponds to $\mathcal{CCC}$ case and has the form $\mathcal{C}_L(\theta_{ab}, \theta_1)\mathcal{C}_R(\theta_1, \theta_2)\mathcal{C}_L(\theta_2, \theta_{ab})$, where $\theta_1 \in [\theta_{ab}, \theta^u_{ab}]$ and $\theta_2 \in [\theta^d_{ab}, \theta_{ab}]$ (see Appendix B).

Finally, for intermediary values of L, (i.e., $484 < L \leq 1,055$ meters) only one of the heading angles θ^u_{ab} and θ^d_{ab} (in our examples, θ^u_{ab}) can be reached by the vessel without "overshooting" the target point. Then, an optimal path corresponds to the $\mathcal{CSCC}$ case and has the form $\mathcal{C}_L(\theta_{ab}, \theta^u_{ab})S_1\mathcal{C}_R(\theta^u_{ab}, \theta_2)\mathcal{C}_L(\theta_2, \theta_{ab})$, where S_1 is a straight line segment with heading θ^u_{ab} and $\theta_2 \in [\theta^d_{ab}, \theta_{ab}]$. (See Appendix B for calculations.)

Our discussion above delivers a *synthesis* of the optimal paths from the configuration (x_s, y_s, θ_s) to (x_t, y_t, θ_t) depending on the position of (x_t, y_t) on the x-axis by dividing the space $[0, \infty)$ into three regions: a $\mathcal{CCC}$-zone, a $\mathcal{CSCC}$-zone, and a $\mathcal{CSCSC}$-zone. This synthesis is illustrated in Figure 32, where dashed lines partition the three regions, and solid curved lines provide an example of an optimal path for each case.

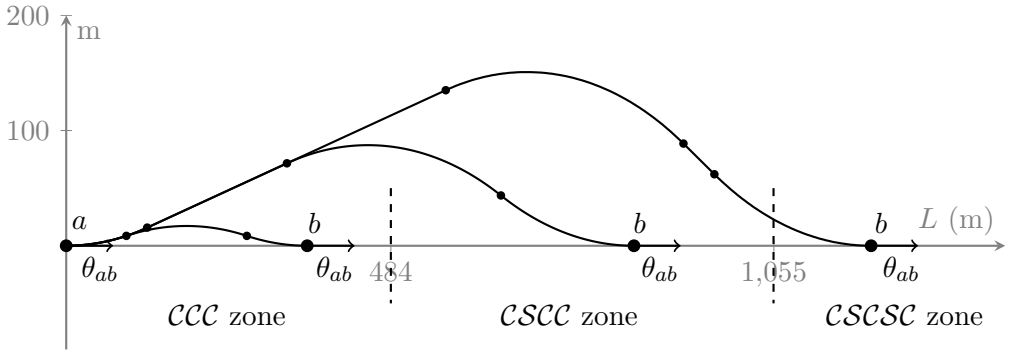

Figure 32: Illustration of the synthesis of the optimal path structure along the x axis and examples of the optimal paths for each scenario.

Next, we compute the travel time along an optimal path for a set of L values and compare them to the travel time along the Dubins path (i.e., straight line). Let $\tau^*(L)$ be the travel time for an optimal path from $s = (0, 0),\ \theta_s = 0°$ to $t = (L, 0),\ \theta_t = 0°$. Table 1 compares the values of $\tau_D(L)$ and $\tau^*(L)$ for different L, highlighting the savings achieved from applying our results (improvement =

$(\tau_D - \tau^*)/\tau_D \cdot 100\%$). We observe that the improvement over the Dubins' path increases up to the limit $(V^* - V(315°))/(V^*)$ which is characterized by the speed along the x-axis $V(315°)$ and the average speed V^* attained by traveling along lines of headings θ^u_{ab} and θ^d_{ab} to reach the same destination (see (Dolinskaya & Smith, 2012) for detailed discussion of this limiting property). The limit is found to be 31.19%, which is in line with our numerical results.

L (m)	200	400	600	1000	2000	5000	10000	100000
$\tau_{\mathbf{D}}$ (s)	32.29	64.58	96.87	161.45	322.9	807.25	1614.49	16144.92
τ^* (s)	29.88	56.02	79.74	124.93	236	569	1124.8	11124
improvement	**7.46%**	**13.25%**	**17.68%**	**22.62%**	**26.91%**	**29.51%**	**30.33%**	**31.10%**

Table 1: Numerical results of the S175 containership example.

5 Conclusion

This paper presents a detailed characterization of a fastest path with bounded curvature where the mobile agent's speed and minimum turning radius are direction-dependent functions. While path finding with curvature constraint is extensively studied in the fields of robotics and UAV routing, this work is the first to characterize an optimal path in a generalized anisotropic medium. One of our key results establishes that there exists an optimal path that is a portion of a path of type $\mathcal{CSCSC}$, where $\mathcal{C}$ denotes a sharpest turn curve and $\mathcal{S}$ a straight line segment. An application of the results to a vessel routing problem in a stationary random seaway illustrates the distinction between our findings and the preceding literature. These numerical results also provide insight to the complexity of the problem and the implementation of the optimal paths. Furthermore, the analysis of a special case (convex speed polar plot) delivers more detailed characterization of an optimal path and an algorithm for constructing such path for given starting and target states of the system.

In the forthcoming work we relax the assumptions of time and space homogeneity. We integrate the results presented here into a dynamic programming model to evaluate time-optimal trajectories in dynamic environments while satisfying the bounded curvature constraint. At the same time, the analytical results of this paper facilitate real-time implementation of the dynamic programming model. In the future, we plan to further study the optimal path characterization to compute a synthesis of the fastest path and to construct an algorithm that implements the results presented in this paper for the non-convex speed polar plots. We plan to analyze more specific structures of the functions $V(\theta)$ and $R(\theta)$ to be able to divide the configuration space into regions reachable by the same optimal path configuration. We also plan to relax Assumption 1 and consider the problems where mobile agent can vary its speed along a path.

A Omitted Proofs

A.1 Proof of Proposition 24

Proof. By symmetry, the proofs for $\mathcal{CCSCSC}$ and $\mathcal{CSCSCC}$ are identical and we thus present only one of these cases. Assume there exists an optimal path which contains a segment of the form $\mathcal{CCSCSC}$.

Define θ_1 and θ_2 to be the headings of the two straight lines L_1 and L_2 in the direction of travel, respectively. Since we assume a structure of an optimal path starts with $\mathcal{CCSCS}$, the optimal path starts with $\mathcal{C}_L(\theta_s, \theta^*_s)$, followed by $\mathcal{C}_R(\theta^*_s, \theta_1)$. Consequently, there exists $\theta_i \in \{\theta_s, \theta_1\}$ such that the headings belonging to $\Theta_L(\theta_i, \theta^*_s) = \Theta_R(\theta^*_s, \theta_i)$ are spanned twice. We want to show that it is not necessary to traverse these two curves and the two straight line segments L_1 and L_2 on the same path. In order to achieve this, we show that we can always perform *feasible-transformations* which either delete all or part of one of the three components (L_1, L_2 and $(\mathcal{C}_L(\theta_i, \theta^*_s), \mathcal{C}_R(\theta^*_s, \theta_i))$ and/or replace one of them by a combination of the other two.

Let us introduce some notation. We divide the interval $[0, 2\pi]$ into four subintervals Θ_I, Θ_{II}, Θ_{III} and Θ_{IV} defined as $\Theta_I = \Theta_L(\theta_i, \theta^*_s)$, $\Theta_{II} = \Theta_R(\theta_i, (\theta^*_s + \pi) \bmod 2\pi)$, $\Theta_{III} = \Theta_L(\theta^*_s, (\theta_i + \pi) \bmod 2\pi)$ and $\Theta_{IV} = \Theta_R((\theta^*_s + \pi) \bmod 2\pi, (\theta_i + \pi) \bmod 2\pi)$ (see Figure 33 for a visual representation). Observe

that from Proposition 19 and the definition of θ_i, the headings θ_1 and θ_2 cannot belong to Θ_I. We also let $\theta_M := \alpha(M)$ be the heading of the displacement M corresponding to $M := \mathcal{C}_L(\theta_i, \theta_s^*) + \mathcal{C}_R(\theta_s^*, \theta_i)$ (see Figure 34). We may assume without loss of generality that $||\Theta_L(\theta_i, \theta_s^*)|| < \pi$ so that $\theta_M \in \Theta(\theta_i, \theta_s^*) = \Theta_I$.

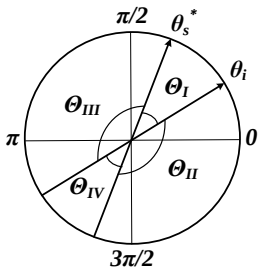

Figure 33: Heading angles intervals Θ_I, Θ_{II}, Θ_{III} and Θ_{IV} displayed on a trigonometric circle.

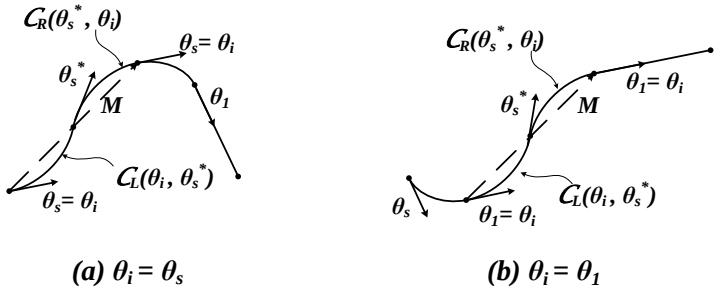

Figure 34: Two possible cases for the value of θ_i: (a) $\theta_i = \theta_s$, (b) $\theta_i = \theta_1$.

The proof of the proposition is done in several steps encompassing all the possible scenarios. In each sub-case, we wish to replace either path segments $\mathcal{C}_L(\theta_i, \theta_s^*) + \mathcal{C}_R(\theta_s^*, \theta_i)$, L_1 or L_2 by shortening or elongating the other two elements, motivated by Observation 15. This is the main argument used in the rest of the proof where in most cases we show that there is a given displacement travelled in two different ways, and then make *feasible-transformation* (rearrangements) of the path segments to simplify the structure of the path.

(i) $\theta_1, \theta_2 \in \Theta_{II}$ **or** $\theta_1, \theta_2 \in \Theta_{III}$**:** The proofs for both cases are identical by switching the roles of L_1 and L_2. In the rest of this sub-case, we consider the setting where $\theta_1, \theta_2 \in \Theta_{II}$. The objective in this case is to replace L_1 by combination of a straight line segment with heading θ_s^* and an elongation of L_2 (see Figure 35).

When $\theta_1, \theta_2 \in \Theta_{II}$, we can write L_1 as a linear combination with positive coefficients of L_2 and any straight line with heading in Θ_I. Furthermore, since we assume that $||\Theta_I|| < \pi$, for any $\theta \in \Theta_I$ the displacement of the segment $\mathcal{C}_L(\theta, \theta_s^*) + \mathcal{C}_R(\theta_s^*, \theta)$ belongs to Θ_I. Recall that a combination of a curve and its reverse curve is symmetrical with respect to the point where the turning direction changes (the point where the two arcs connect). For any $\theta \in \Theta_I$, let $P_\theta := \mathcal{C}_L(\theta, \theta_s^*) + \mathcal{C}_R(\theta_s^*, \theta)$ be the displacement obtained by following the curve $\mathcal{C}_L(\theta, \theta_s^*)$ and the corresponding time reversed curve $\mathcal{C}_R(\theta_s^*, \theta)$.

We have for instance $P_{\theta_{s^*}} = \vec{0}$ and $P_{\theta_i} = M$. In fact, in order to condense the notation, let us consider the function $P(\lambda)$ defined on $[0, 1]$ which assigns to $\lambda \in [0, 1]$ the displacement $P_{\theta_{s^*} + \lambda(\theta_i - \theta_{s^*})}$: $P : \lambda \in [0, 1] \longrightarrow P_{\theta_{s^*} + \lambda(\theta_i - \theta_{s^*})} \in \mathbb{R}^2$. The notation here can be slightly abusive depending on the values of θ_s^* and θ_i, it might need to be adjusted in some cases to ensure that as λ goes from 0 to 1 we span the set $\Theta_R(\theta_s^*, \theta_i)$. We thus have $P(0) = \vec{0}$ and $P(1) = M$. Since $P(0) = \vec{0}$, we may also write $P(0) + \alpha_0 L_2 = \beta_0 L_1$ with $\alpha_0 = \beta_0 = 0$. We use this trivial expression to illustrate the

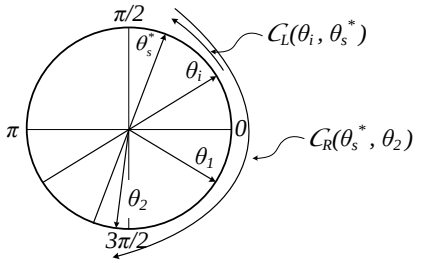

Figure 35: Case (i) Representation of the turns and spanned headings on a trigonometric circle when $\theta_1, \theta_2 \in \Theta_{II}$.

fact that we wish to match the displacement obtained by a portion of L_1 with the displacement obtained by a portion of the two curves $\mathcal{C}_L(\theta_i, \theta_s^*) + \mathcal{C}_R(\theta_s^*, \theta_i)$ (which corresponds to $P(\lambda)$ for some $\lambda \in [0,1]$) and a portion of L_2. From the continuity assumptions of $R(\theta)$ and $V(\theta)$, the function $\lambda \mapsto \|P(\lambda)\|$ is continuous on $[0,1]$ and we have $\|P(0)\| = 0$ and $\|P(1)\| = \|M\|$. This guarantees that there exists $\hat{\lambda}$ such that for all $\lambda \in [0, \hat{\lambda}]$, we can write $P(\lambda) + \alpha_\lambda L_2 = \beta_\lambda L_1$ as desired. Indeed, as long as $\|P(\lambda)\| \leq \min\{\|L_1\|, \|L_2\|\}$, we may form a triangle whose sides are $P(\lambda)$, a portion of L_1 and a portion of L_2. We illustrate this fact in Figure 36 where we draw the two curves $\mathcal{C}_L(\theta_i, \theta_s^*) + \mathcal{C}_R(\theta_s^*, \theta_i)$, L_1 and L_2 (in (a)) and then rearrange the pieces in (b) and (c) to make such property apparent.

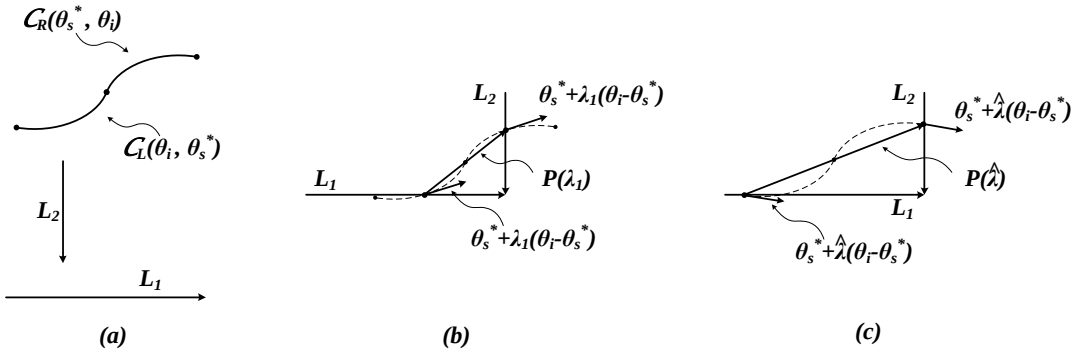

Figure 36: Case (i) $\theta_1, \theta_2 \in \Theta_{II}$ or $\theta_1, \theta_2 \in \Theta_{III}$: (a) curves $\mathcal{C}_L(\theta_i, \theta_s^*) + \mathcal{C}_R(\theta_s^*, \theta_i)$, L_1 and L_2 drawn individually (b,c) rearrangements of the pieces to realize the same displacement using some $\lambda_1 \in [0, \hat{\lambda}]$ and $\hat{\lambda} \in [0,1]$.

We have so far shown that there exists a set of headings corresponding to $\theta_{s^*} + \lambda(\theta_i - \theta_{s^*})$ for $\lambda \in [0, \hat{\lambda}]$ for which we can write $P(\lambda) + \alpha_\lambda L_2 = \beta_\lambda L_1$. In other words there exists a set of headings for which the same displacement $P(\lambda) + \alpha_\lambda L_2 = \beta_\lambda L_1$ is realized in two different ways along the optimal path, once as a portion of L_1 and once as a combination of the two curves $\mathcal{C}_L(\theta_{s^*} + \lambda(\theta_i - \theta_{s^*}), \theta_s^*) + \mathcal{C}_R(\theta_s^*, \theta_{s^*} + \lambda(\theta_i - \theta_{s^*}))$ and a portion of L_2. From Observation 15, we know that the travel times given by each of these two components must be the same.

We then know that if we fixed $\lambda \in [0, \hat{\lambda}]$, we could replace $\beta_\lambda L_1$ by $P(\lambda) + \alpha_\lambda L_2$. However this would only replace a portion of L_1, not necessarily all of it, and insert new curves. Instead, we want to replace the entire segment L_1 by something that would yield a simpler structure to the path. In order to do this, we observe that for any $\lambda \in [0, \hat{\lambda}]$, the paths given by a) following a straight line with heading θ_1 and b) following a straight line with heading $\theta_{s^*} + \lambda(\theta_i - \theta_{s^*})$ and then a straight line with heading θ_2, take the same travel time for the same displacement. Otherwise there would exist a subset of $[0, \hat{\lambda}]$ for which the travel time of $P(\lambda) + \alpha_\lambda L_2$ would be either higher

or lower than the travel time of $\beta_\lambda L_1$, which would contradict Observation 15. In particular, this holds true for $\lambda = 0$, i.e. $\theta_{s^*} + \lambda(\theta_i - \theta_{s^*}) = \theta_s^*$, and we can erase L_1 entirely from the optimal path and substitute it by inserting a straight line with heading θ_s^* and elongating L_2 (see Figure 37 for an example). This results in transforming the original segment into as fast a segment in which the structure $\mathcal{CCSCSC}$ has become $\mathcal{CSCSC}$ as desired.

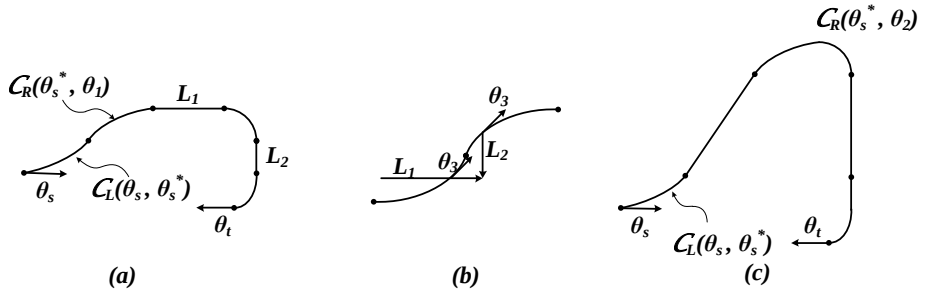

Figure 37: Case (i) $\theta_1, \theta_2 \in \Theta_{II}$ or $\theta_1, \theta_2 \in \Theta_{III}$: (a) original path, (b) zoomed in portions of interest, (c) new optimal path.

(ii) $\theta_1 \in \Theta_{II}$ **and** $\theta_2 \in \Theta_{III}$**:** In this case we want to write the curves' displacement M as a linear combination of L_1 and L_2: $M = \alpha_1 L_1 + \alpha_2 L_2$. We need however to distinguish two subcases which yield different signs for the coefficients: *a)* $\Theta_L(\theta_2, \theta_1) > \pi$ for which $\alpha_1, \alpha_2 > 0$, *b)* $\Theta_L(\theta_2, \theta_1) < \pi$ for which $\alpha_1, \alpha_2 < 0$ (see Figure 38). In the former we transform the path into an equally fast path of the desired structure, and we show that the latter cannot be optimal. Note that we exclude the case $\theta_1 = \theta_2 + \pi \bmod 2\pi$ since it trivially reduces to a path that contains only one straight line segment.

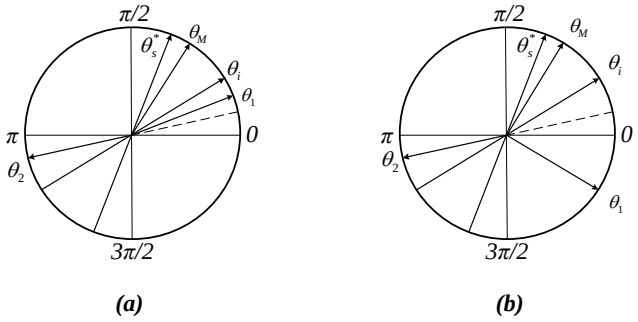

Figure 38: Case (ii) $\theta_1 \in \Theta_{II}$ and $\theta_2 \in \Theta_{III}$: Representation of the headings on a trigonometric circle for a) $\Theta_L(\theta_2, \theta_1) > \pi$ and b) $\Theta_L(\theta_2, \theta_1) < \pi$.

a) $\Theta_L(\theta_2, \theta_1) > \pi$**:** If $\Theta_L(\theta_2, \theta_1) > \pi$, then we can write $M = \alpha_1 L_1 + \alpha_2 L_2$ with $\alpha_1, \alpha_2 > 0$. Similarly to the first subcase (i), we are traversing the same displacement twice along an optimal path with two different components $\mathcal{C}_L(\theta_i, \theta_s^*) + \mathcal{C}_R(\theta_s^*, \theta_i)$ and $\alpha_1 L_1 + \alpha_2 L_2$. From Observation 15, both travels must be equally fast, and we can replace the two curves $\mathcal{C}_L(\theta_i, \theta_s^*) + \mathcal{C}_R(\theta_s^*, \theta_i)$, corresponding to the displacement M, by the equivalent displacement $\alpha_1 L_1 + \alpha_2 L_2$, which corresponds to elongating the straight line segments L_1 and L_2. In doing so, we change from a structure $\mathcal{CCSCSC}$ to a structure $\mathcal{CSCSC}$.

b) $\Theta_L(\theta_2, \theta_1) < \pi$**:** We show that this case is not optimal. If $\Theta_L(\theta_2, \theta_1) < \pi$, then we can write $M = \alpha_1 L_1 + \alpha_2 L_2$ with $\alpha_1, \alpha_2 < 0$. Suppose $\alpha_1, \alpha_2 \leq -1$, then L_1 and L_2 are long enough to eliminate the two curves $\mathcal{C}_L(\theta_i, \theta_s^*)$ and $\mathcal{C}_R(\theta_s^*, \theta_i)$ by shortening L_1 and L_2 (see Figure 39).

However, the resulting path would be faster than the original path since we eliminate segments of the path, violating the optimality assumption. This setting hence violates optimality assumption.

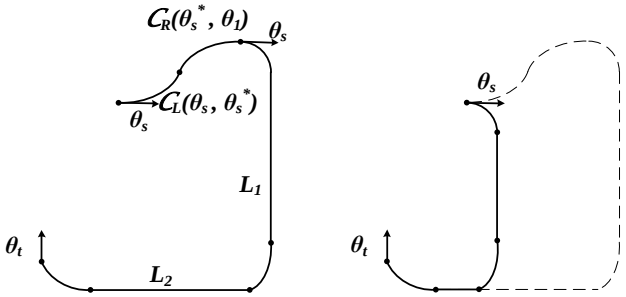

Figure 39: Case (ii) b) where $\alpha_1, \alpha_2 \leq -1$: original path (left) and shortened path (right).

Similarly, if $\alpha_1 \in (-1, 0)$ or $\alpha_2 \in (-1, 0)$ and we cannot completely eliminate the two curves $\mathcal{C}_L(\theta_i, \theta_s^*)$ and $\mathcal{C}_R(\theta_s^*, \theta_i)$ by reducing the lines L_1 and L_2, we show that it would still be possible to eliminate parts of the path, again violating the optimality assumption.

Proceeding in a similar manner to scenario (i), there exists $\theta_4 \in \Theta_L(\theta_i, \theta_s^*)$ and $\beta < 0$ such that either $\mathcal{C}_L(\theta_4, \theta_s^*) + \mathcal{C}_R(\theta_s^*, \theta_4) = L_1 + \beta L_2$ or $\mathcal{C}_L(\theta_4, \theta_s^*) + \mathcal{C}_R(\theta_s^*, \theta_4) = L_2 + \beta L_1$. In other words, there is a way to express a portion of the two curves as a combination of either L_1 and a portion of L_2, or L_2 and a portion of L_1. In either cases, we can *feasibly-transform* the path by eliminating the curves $\mathcal{C}_L(\theta_4, \theta_s^*)$ and $\mathcal{C}_R(\theta_s^*, \theta_4)$ by omitting either L_1 or L_2 and shortening the other one. This also yields a faster path, contradicting the assumption that the original path is optimal (see Figure 40). Intuitively it makes sense that such combination would not be optimal since the two curves have a displacement that is in the 'opposite' direction to the straight line segments, corresponding to going backwards and then forward again.

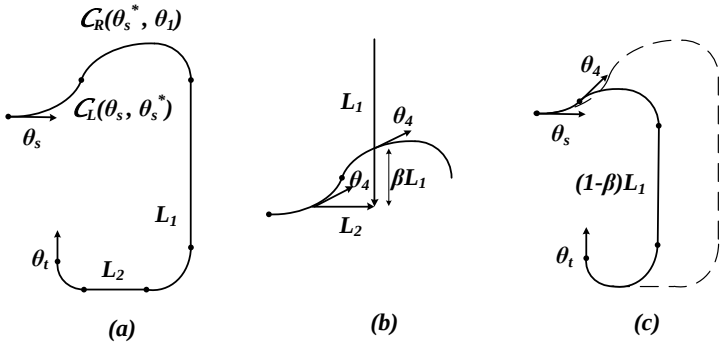

Figure 40: Case (ii) b) where $\alpha_1 \in (-1, 0)$ or $\alpha_2 \in (-1, 0)$: original path (left) and improved path (right).

To summarize case (ii), we established that if a) $\Theta_L(\theta_2, \theta_1) > \pi$, there exists a path with the same travel time that does not contain a segment of the form $\mathcal{CCSCSC}$; and if b) $\Theta_L(\theta_2, \theta_1) < \pi$, an optimal path cannot have the structure $\mathcal{CCSCSC}$.

We can now move to the third and final subcase of the proof.

(iii) $\theta_1 \in \Theta_{IV}$ **or** $\theta_2 \in \Theta_{IV}$ **(or both):** This is a mixed case in which we can apply the results from first two subcases. Indeed, the idea is to define an alternate value θ_i' for θ_i so that if we redefine the regions Θ_I, Θ_{II}, Θ_{III} and Θ_{IV} using θ_i' instead of θ_i, we find ourselves in the settings of either case (i) or case (ii). Case (iii) encompasses three subcases: (a) $\theta_1 \in \Theta_{IV}$ and $\theta_2 \notin \Theta_{IV}$, (b) $\theta_1 \notin \Theta_{IV}$

and $\theta_2 \in \Theta_{IV}$, (c) $\theta_1 \in \Theta_{IV}$ and $\theta_2 \in \Theta_{IV}$. Because the proofs for the three subcases are similar, we only carry out the proof for subcase (c).

Suppose $\theta_1 \in \Theta_{IV}$ and $\theta_2 \in \Theta_{IV}$. We then let θ_i' be an arbitrary heading in the set $\Theta_L(\theta_1 + \pi \bmod 2\pi, \theta_s^*)$ and redefine the regions Θ_I, Θ_{II}, Θ_{III} and Θ_{IV} using θ_i' instead of θ_i. This transformation modifies the setting into that of case (i) and we may then apply the methods presented there. (See Figure 41).

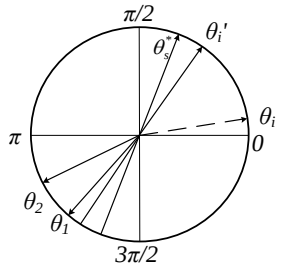

Figure 41: Case (iii) $\theta_1 \in \Theta_{IV}$ or $\theta_2 \in \Theta_{IV}$ (or both): representation of the headings on a trigonometric circle.

□

A.2 Proof of Theorem 27

Proof. Allow $t(p)$ denote the travel time along path p. To compute $t(p^*)$, apply polygonal approximation to the path $p^* : [0,1] \to \mathbb{R}^2$. Choose an arbitrary partition Π of the interval $[0,1]$, i.e., let $\Pi = (r_0, r_1, r_2, ..., r_k)$ such that $0 = r_0 < r_1 < r_2 < ... < r_{k-1} < r_k = 1$. Let mesh $|\Pi|$ be the maximum length $r_i - r_{i-1}$ of a subinterval of Π, that is, $|\Pi| = \max_{1 \le i \le k}\{r_i - r_{i-1}\}$. Then Π defines a polygonal approximation to p^*, i.e., the polygonal arc from $p^*(0) = a$ to $p^*(1) = b$ having successive vertices $p^*(r_0)$, $p^*(r_1)$, ..., $p^*(r_k)$ (see Figure 42).

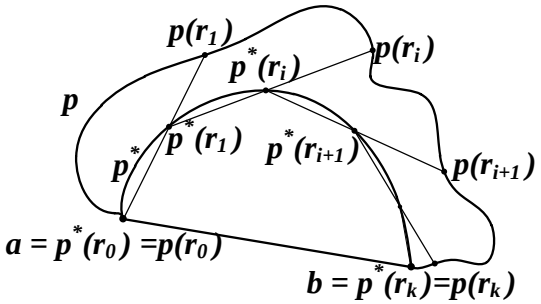

Figure 42: Illustration of the proof of Theorem 27.

The travel time along a polygonal approximation of the path can be written as $\eta(p^*, \Pi) = \sum_{i=1}^{k} \tau(p^*(r_{i-1}), p^*(r_i))$, where $\tau(c,d)$ denotes the travel time along a straight line segment cd. As $|\Pi|$ approaches zero, the number of vertices increases and the polygonal approximation in the limit is equivalent to path p^*; thus their travel times are also equivalent to the path (this follows from the assumption that path p^* is rectifiable). Given this,

$$t(p^*) = \lim_{|\Pi| \to 0} \eta(p^*, \Pi). \tag{34}$$

Next, we compare $t(p^*)$ to $t(p)$. Since S_{p^*} is convex and $S_{p^*} \subseteq S_p$, a line containing segment $p^*(r_i)p^*(r_{i+1})$ for any $0 \leq i < k$ has to intersect curve p at least once. We let $p(r_{i+1})$ denote the intersection point closest to point $p^*(r_{i+1})$ and such that the line segment $p^*(r_i)p(r_{i+1})$ contains point $p^*(r_{i+1})$. Then, if we let $t(p(r_i, r_{i+1}))$ represent the travel time along a segment of the curve p between the points $p(r_i)$ and $p(r_{i+1})$, Lemma 26 implies the following inequalities for $i \in [0, ..., k-1]$ (see Figure 42).

$$\begin{aligned} \tau(p^*(r_i), p(r_i)) + t(p(r_i, r_{i+1})) &\geq \tau(p^*(r_i), p(r_{i+1})) \\ &= \tau(p^*(r_i), p^*(r_{i+1})) + \tau(p^*(r_{i+1}), p(r_{i+1})). \end{aligned} \tag{35}$$

Note that $p^*(r_0) = p(r_0)$ and $p^*(r_k) = p(r_k)$ implying that $\tau(p^*(r_0), p(r_0)) = \tau(p^*(r_k), p(r_k)) = 0$. Summing inequalities (35) for all $i \in [0, ..., k-1]$ results in the following inequality,

$$\begin{aligned} \Sigma_{i=0}^{k-1} t(p(r_i, r_{i+1})) &\geq \Sigma_{i=0}^{k-1} \tau(p^*(r_i), p^*(r_{i+1})), \\ t(p) &\geq \eta(p^*, \Pi). \end{aligned} \tag{36}$$

Combining (34) and inequality (36), we obtain the desired result $t(p) \geq t(p^*)$.

□

A.3 Proof of Theorem 30

Proof. Consider a *relaxed-optimal sub-path* that contains two directed line segments D_1 and D_2 with the distinct heading angles θ_1 and θ_2, respectively. Our goal is to construct an alternative path that replaces D_1 and D_2 as part of the given sub-path, contains at most one line segment, and has a travel time no greater than the sum of travel times for D_1 and D_2. The total displacement for the alternative path must equal $D_1 + D_2$. Furthermore, the total heading change along the alternative path has to equal zero. We construct an alternative path replacing $\frac{1}{2}D_1$ and $\frac{1}{2}D_2$ parts of the path without the restriction on the total heading change. Property 11 implies that by replacing the second part of $\frac{1}{2}(D_1 + D_2)$ with the time-reversed path results in the proper alternative path and negates the overall heading change.

Continuity of the heading angle along a feasible path implies that either $\mathcal{C}_R(\theta_1, \theta_2)$ or $\mathcal{C}_L(\theta_1, \theta_2)$ has to be part of the path containing D_1 and D_2. Without loss of generality, assume $\mathcal{C}_R(\theta_1, \theta_2)$ is part of the path. Consequently, any proposed alternative path has to start with the heading angle in $\Theta_R(\theta_1, \theta_2)$ to ensure its feasibility.

Case 1: $\alpha(D_1 + D_2) \in \Theta_R(\theta_1, \theta_2)$.
When $\alpha(D_1 + D_2) \in \Theta_R(\theta_1, \theta_2)$, including the straight line segment equal to the displacement $D_1 + D_2$ is feasible, and we can replace D_1 and D_2 by that single line segment. Lemma 26 states that the travel time for the resulting path is not greater than for the original path, thus maintaining its optimality.

Case 2: $\alpha(D_1 + D_2) \notin \Theta_R(\theta_1, \theta_2) \Rightarrow \alpha(D_1 + D_2) \in \Theta_L(\theta_1, \theta_2)$.
Since $\alpha(D_1 + D_2) \in \Theta_L(\theta_1, \theta_2)$, we know that $\|\Theta_L(\theta_1, \theta_2)\| \leq \pi$. Let $\theta' := \alpha(D(\mathcal{C}_L(\theta_1, \theta_2)))$, then Property 8 implies $\theta' \in \Theta_L(\theta_1, \theta_2)$.

Due to the symmetry of $\mathcal{C}_R(\theta_2, \theta_1)$ and $\mathcal{C}_L(\theta_1, \theta_2)$, we assume $\alpha(D_1 + D_2) \in \Theta_L(\theta_1, \theta')$ as opposed to $\Theta_L(\theta', \theta_2)$, without loss of generality. Let the curve $\mathcal{C}_L(\theta_1, \theta_2)$ and the displacement vector $\frac{1}{2}(D_1 + D_2)$ start at the same point, denoted by a. Then, the curve must intersect the line containing the displacement vector $\frac{1}{2}(D_1 + D_2)$, and we call the intersection point d. Let $\theta_d \in \Theta_L(\theta_1, \theta_2)$ denote the heading angle of the curve $\mathcal{C}_L(\theta_1, \theta_2)$ at point d, that is, $\frac{1}{2}(D_1 + D_2) || D(\mathcal{C}_L(\theta_1, \theta_d)$. Then, if $c := a + \frac{1}{2}(D_1 + D_2)$, either $d \in ac$ or $c \in ad$, and we consider the following two subcases separately.

Case 2a: $d \in ac$ (see Figure 43).
We can complete the path from a to c by adding the line segment dc to the curve $\mathcal{C}_L(\theta_1, \theta_d)$. Note that since $\Theta_L(\theta_1, \theta_d) \subseteq \Theta_L(\theta_1, \theta_2)$ and $\|\Theta_L(\theta_1, \theta_2)\| \leq \pi$, Property 8 implies that $\alpha(dc) = \alpha(D(\mathcal{C}_L(\theta_1, \theta_d))) \in \Theta_L(\theta_1, \theta_d)$. The resulting path consists of $\mathcal{C}_L(\theta_1, \alpha(dc))$ followed by the line segment dc and then the curve $\mathcal{C}_L(\alpha(dc), \theta_d)$. It is a convex path enclosed by a path $\frac{1}{2}D_1$ followed by $\frac{1}{2}D_2$, and Theorem 27 states that its travel time satisfies the requirements to maintain the optimality of the proposed path.

Case 2b: $c \in ad$ (see Figure 44).
Let point b denote the end of segment $\frac{1}{2}D_1$ starting at a, that is, $b = a + \frac{1}{2}D_1$. Then $bc = \frac{1}{2}D_2$. We also let $\mathcal{C}_a$ denote the curve $\mathcal{C}_L(\theta_1, \theta_2)$ starting at a. The fact that $c \in ad$ and $\alpha(ac) \in \Theta_L(\theta_1, \theta')$ implies that curve $\mathcal{C}_a$ intersects bc, since it does not intersect ac and it cannot intersect ab (Property 9).

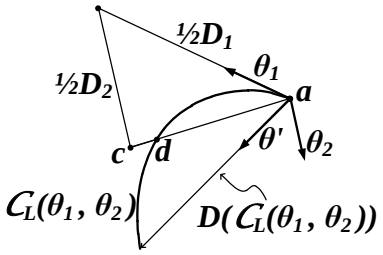

Figure 43: Illustration of Theorem 30 Case 2a.

Similarly, we let $\mathcal{C}_c$ to denote the curve $\mathcal{C}_L(\theta_1, \theta_2)$ ending at point c. Curve $\mathcal{C}_c$ must intersect ab and curve $\mathcal{C}_a$, we call $e := \mathcal{C}_a \bigcap \mathcal{C}_c$, and the intersection point must lie inside the triangle defined by vertexes abc. Then, the alternative proposed path is to follow curve $\mathcal{C}_a$ from point a to point e and then follow curve $\mathcal{C}_c$ from e to c. The constructed path is a convex path enclosed by a path $\frac{1}{2}D_1$ followed by $\frac{1}{2}D_2$, and Theorem 27 states that its travel time satisfies the requirements to maintain the optimality of the proposed path.

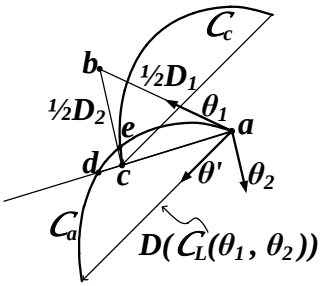

Figure 44: Illustration of Theorem 30 Case 2b.

□

A.4 Proof of Proposition 31

Proof. Proposition 20 states that there exists a *relaxed-optimal sub-path* such that the only curves it contains are $\{\mathcal{C}_L(\theta_s, \theta_s^*), \mathcal{C}_R(\theta_s^*, \theta_s)\}$ and $\{\mathcal{C}_R(\theta_t, \theta_t^*), \mathcal{C}_L(\theta_t^*, \theta_t)\}$. And Theorem 30 proves that we can have a *relaxed-optimal sub-path* with at most one line segment. The two propositions do not contradict each other, and we can conclude that there exists a *relaxed-optimal sub-path* that can only contain the given two pairs of curves and a single line segment. We are left to prove that the heading angle of the line can only be equal to θ_s^* or θ_t^*, instead of the *interior* defined as $\Theta_R(\theta_s^*, \theta_t^*)/\{\theta_s^*, \theta_t^*\}$.

Consider a path containing line segment D_1 with the corresponding heading angle θ_1, such that $\theta_1 \in \Theta_R(\theta_s^*, \theta_t^*)/\{\theta_s^*, \theta_t^*\}$. Since $\|\Theta_R(\theta_s^*, \theta_t^*)\| \leq 2\pi$, either $\|\Theta_R(\theta_s^*, \theta_1)\| \leq \pi$ or $\|\Theta_R(\theta_1, \theta_t^*)\| \leq \pi$. Due to the symmetry of the argument, we assume $\|\Theta_R(\theta_1, \theta_t^*)\| \leq \pi$, without loss of generality. Then, our goal is to construct an alternative path with a travel time not greater than the current path, and such that the slope of an alternative line segment has a heading angle equal to θ_s^* or θ_t^*. Note that θ_s^* and θ_t^* are not the specific angle values, but notation used to denote the *boundaries* of the set of headings spanned by a path.

Employing Property 14, consider a part of the path consisting of D_1 and $\mathcal{C}_R(\theta_1, \theta_t^*)$ accompanied by $\mathcal{C}_L(\theta_t^*, \theta_1)$ that is arranged as follows (see Figure 45). Let curve $\mathcal{C}_a$ denote a curve $\mathcal{C}_R(\theta_1, \theta_t^*)$ starting at some point a and let point b denote the end of $\mathcal{C}_a$, that is, $b = a + D(\mathcal{C}_a)$. The line segment D_1 is assumed to start at point b and end at point c, where $c = b + D_1$. Finally, a curve denoted by $\mathcal{C}_c$ is the

curve $\mathcal{C}_L(\theta_t^*, \theta_1)$ starting at point c and ending at point d. We let point e denote the midpoint of the line segment bc.

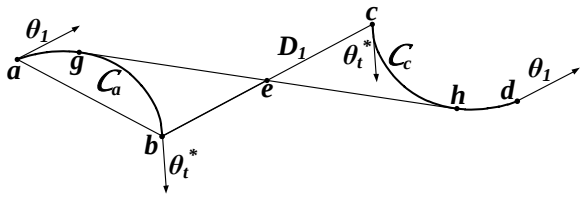

Figure 45: Illustration of Proposition 31 proof.

Since $D(\mathcal{C}_a) \in \Theta_R(\theta_1, \theta_t^*)$, the curve $\mathcal{C}_a$ and line segment ab enclose a convex set, and point e lies outside this set. Then, we construct two tangent lines to this convex set passing through point e and one of those lines is tangential to curve $\mathcal{C}_a$. We let point g denote this tangential point and $\theta_g \in \Theta(\theta_1, \theta_t^*)$ be the slope of the tangent line ge, which is also the heading angle of the curve $\mathcal{C}_a$ at point g. Note that the symmetry of curves $\mathcal{C}_a$ and $\mathcal{C}_c$ relative to point e implies that the line containing segment ge is also tangent to curve $\mathcal{C}_c$ at a point we denote by h. The symmetry also implies that the heading angle of the curve $\mathcal{C}_c$ at point h is equal to θ_g. Then, the part of the path consisting of D_1, $\mathcal{C}_R(\theta_1, \theta_t^*)$ and $\mathcal{C}_L(\theta_t^*, \theta_1)$ can be replaced by a curve $\mathcal{C}_R(\theta_1, \theta_g)$, the directed line segment gh, and curve $\mathcal{C}_L(\theta_g, \theta_1)$. Subsequently, heading θ_g becomes the new θ_t^*.

Note that since we replace $\mathcal{C}_R(\theta_g, \theta_t^*)$, $\mathcal{C}_L(\theta_t^*, \theta_g)$ and D_1 by a straight line segment with the equivalent displacement, Lemma 26 ensures that the alternative path will have a travel time no greater than the original path, thus maintaining its *relaxed-optimality*. □

A.5 Proof of Proposition 32

Proof. Proposition 31 states that there exists a *relaxed-optimal sub-path* that can only contain the curve pairs $\{\mathcal{C}_L(\theta_s, \theta_s^*), \mathcal{C}_R(\theta_s^*, \theta_s)\}$ and $\{\mathcal{C}_R(\theta_t, \theta_t^*), \mathcal{C}_L(\theta_t^*, \theta_t)\}$, and the straight line segment D_1 with the heading angle either equal to θ_s^* or θ_t^*. We show that there exists a *relaxed-optimal sub-path* that would not contain all three components.

Consider a path containing $\mathcal{C}_L(\theta_s, \theta_s^*)\mathcal{C}_R(\theta_s^*, \theta_s)$, $\mathcal{C}_R(\theta_t, \theta_t^*)\mathcal{C}_L(\theta_t^*, \theta_t)$ and a straight line segment D_1, where $\theta_s^* \neq \theta_s$ and $\theta_t^* \neq \theta_t$. Due to the symmetry of the discussion, we assume that the heading angle $\alpha(D_1)$ is equal to θ_t^*, without loss of generality. Employing Property 11, we consider one half of the path that consists of curve $\mathcal{C}_R(\theta_t, \theta_t^*)$, curve $\mathcal{C}_R(\theta_s^*, \theta_s)$, and line segment $\frac{1}{2}D_1$. Our goal is to replace this part of the path with either two sharpest turn curves or one curve and a line segment. Then, implementation of a time reversed path for the second half delivers the necessary results.

Let point a denote the start point of curve $\mathcal{C}_R(\theta_t, \theta_t^*)$, and point b denote the curve's end point. Then, we assume the line segment $\frac{1}{2}D_1$ starts at b and ends at $c = b + \frac{1}{2}D_1$. Finally, we assume $\mathcal{C}_R(\theta_s^*, \theta_s)$ starts at point c and ends at point d. Note that the line segment ad is equal to $\frac{1}{2}D_{Rt}$, implying that $\alpha(ad) \in \Theta_L(\theta_s, \theta_t) = \Theta_R(\theta_t, \theta_s)$. Next, we consider all possible scenarios of the current half-path and prove the proposition for each case individually.

Case 1: Curves $\mathcal{C}_R(\theta_t, \theta_t^*)$ and $\mathcal{C}_R(\theta_s^*, \theta_s)$ intersect at some point e (see Figure 46).
Consider an alternative path consisting of only two curves: part of the curve $\mathcal{C}_R(\theta_t, \theta_t^*)$ between points a and e, followed by part of the curve $\mathcal{C}_R(\theta_s^*, \theta_s)$ between points e and d. Because the proposed path is part of the original path, its travel time has to be less than or equal to the original travel time.

Case 2: Curve $\mathcal{C}_R(\theta_t, \theta_t^*)$ intersects itself (see Figure 47).
We assume that point d does not lie inside the region enclosed by the loop of curve $\mathcal{C}_R(\theta_t, \theta_t^*)$, otherwise curves $\mathcal{C}_R(\theta_t, \theta_t^*)$ and $\mathcal{C}_R(\theta_s^*, \theta_s)$ have to intersect corresponding to Case 1. Then, there exists at least one line tangent to curve $\mathcal{C}_R(\theta_t, \theta_t^*)$ and passing through point d. Let e denote the tangent point of the line to the curve $\mathcal{C}_R(\theta_t, \theta_t^*)$, such that the heading of the curve at that point is equal to $\alpha(ed)$. Consider an alternative path consisting of only one arc and a line segment: part of the curve $\mathcal{C}_R(\theta_t, \theta_t^*)$ between points a and e and a straight line segment ed. Since we replace part of the original path with a straight

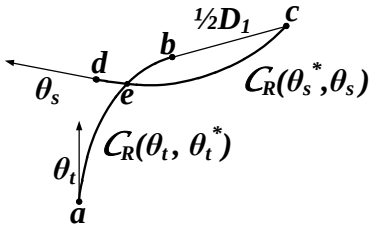

Figure 46: Illustration of Proposition 32 Case 1.

line segment, Lemma 26 implies that travel time of the alternative path is not greater than that of the original path.

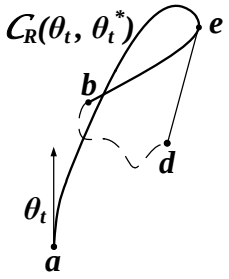

Figure 47: Illustration of Proposition 32 Case 2.

Case 3: $\alpha(cd) \in \Theta_L(\theta_t^*, \theta_t^* + \pi)$ (see Figure 48).
There exists a line segment ed that is tangent to curve $\mathcal{C}_R(\theta_t, \theta_t^*)$ at point e, such that the heading of the curve at that point is equal to $\alpha(ed)$. We construct an alternative path containing one curve an a line segment as discussed in Case 2.

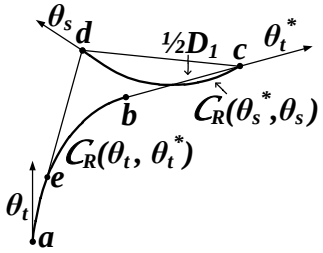

Figure 48: Illustration of Proposition 32 Case 3.

Case 4: $\alpha(cd) \in \Theta_R(\theta_t^*, \theta_t^* + \pi)$.
A curve $\mathcal{C}_R(\theta_t^*, \theta_s)$ starting at point b must either intersect the line segment bd or curve $\mathcal{C}_R(\theta_s^*, \theta_s)$, before a possible intersection with the line segment bc.

Case 4a: Curve $\mathcal{C}_R(\theta_t^*, \theta_s)$ starting at point b intersects line segment bd (see Figure 49).
There exists a line segment ed that is tangent to curve $\mathcal{C}_R(\theta_t^*, \theta_s)$ at point e, such that the heading of the curve at that point is equal to $\alpha(ed)$. Consider an alternative path consisting of a single curve and a line segment: part of the curve $\mathcal{C}_R(\theta_t, \theta_s)$ between points a and e, followed by a straight line segment

ed. Theorem 27 implies that travel time of the alternative path is not greater than that of the original path.

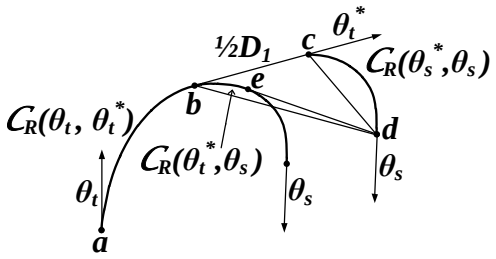

Figure 49: Illustration of Proposition 32 Case 4a.

Case 4b: Curve $\mathcal{C}_R(\theta_t^*, \theta_s)$ starting at point b intersects curve $\mathcal{C}_R(\theta_s^*, \theta_s)$ (see Figure 50).
Let e denote the intersection point of the two curves. Then a path consisting of two curves: a part of the curve $\mathcal{C}_R(\theta_t, \theta_s)$ between points a and e, and a part of the curve $\mathcal{C}_R(\theta_s^*, \theta_s)$ between points e and d, has a travel time no greater than the original path (Theorem 27). Note that the set of heading angles spanned by the two new curves cannot intersect. □

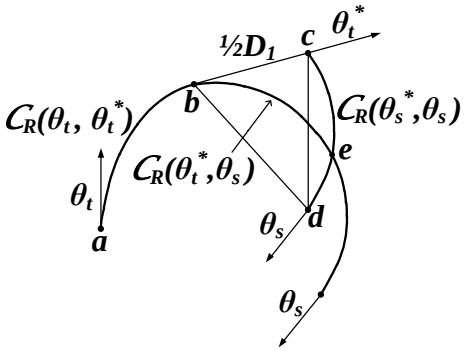

Figure 50: Illustration of Proposition 32 Case 4b.

B Supporting Calculations for Numerical Results in Section 4

B.1 Displacement Vectors Calculation

In order to be able to implement our results, we need to compute the displacement vector of the mobile agent along a path. The optimal paths derived in this paper are composed of two types of path segments: (1) straight-line segments, denoted by $\mathcal{S}$, and (2) sharpest turn curves, $\mathcal{C}$. Thus, we only need to compute the displacements for these two types of segments. Then, the additive property enables us to find the displacement of an optimal path by adding the displacements of the individual path segments.

Straight-line displacement, $D(S)$: Let S be a straight-line segment from s_1 to s_2, with length $||S||$ and direction denoted by θ_S. The displacement of the agent traversing S, $D(S)$, can be found as:

$$D(S) = \begin{pmatrix} ||S|| \cos\theta_S \\ ||S|| \sin\theta_S \end{pmatrix}.$$

Sharpest turn curve displacement, $D(\mathcal{C})$: A sharpest turn curve $\mathcal{C}_k(\theta_1, \theta_2)$ for $k \in \{L, R\}$ can correspond to either a right-hand or a left-hand turn. Then, for given initial and final headings, θ_1 and θ_2, respectively, the ensuing displacements differ for a mobile agent traveling along $\mathcal{C}_L(\theta_1, \theta_2)$ versus $\mathcal{C}_R(\theta_1, \theta_2)$. Thus, we treat each case separately. (For notation consistency, we let $\theta_1, \theta_2 \in S^1$.)

Left turn $\mathcal{C}_L(\theta_1, \theta_2)$: The displacement $D\left(\mathcal{C}_L(\theta_1, \theta_2)\right)$ achieved by a left-hand sharpest turn curve is given by:

$$D\left(\mathcal{C}_L(\theta_1, \theta_2)\right) = \begin{cases} \begin{pmatrix} \int_{\theta_1}^{\theta_2} R(\theta)\cos\theta d\theta \\ \int_{\theta_1}^{\theta_2} R(\theta)\sin\theta d\theta \end{pmatrix}, & \theta_1 \leq \theta_2 \\ \begin{pmatrix} \int_{\theta_1}^{2\pi} R(\theta)\cos\theta d\theta + \int_{0}^{\theta_2} R(\theta)\cos\theta d\theta \\ \int_{\theta_1}^{2\pi} R(\theta)\sin\theta d\theta + \int_{0}^{\theta_2} R(\theta)\sin\theta d\theta \end{pmatrix}, & \theta_1 > \theta_2. \end{cases}$$

Right turn $\mathcal{C}_R(\theta_1, \theta_2)$: The displacement $D\left(\mathcal{C}_R(\theta_1, \theta_2)\right)$ achieved by a right-hand sharpest turn curve is given by:

$$D\left(\mathcal{C}_R(\theta_1, \theta_2)\right) = \begin{cases} \begin{pmatrix} \int_{\theta_2}^{\theta_1} R(\theta)\cos\theta d\theta \\ \int_{\theta_2}^{\theta_1} R(\theta)\sin\theta d\theta \end{pmatrix}, & \theta_1 > \theta_2 \\ \begin{pmatrix} \int_{\theta_2}^{2\pi} R(\theta)\cos\theta d\theta + \int_{0}^{\theta_1} R(\theta)\cos\theta d\theta \\ \int_{\theta_2}^{2\pi} R(\theta)\sin\theta d\theta + \int_{0}^{\theta_1} R(\theta)\sin\theta d\theta \end{pmatrix}, & \theta_1 \leq \theta_2. \end{cases}$$

Remark.

- *Note that in the case when the axes are rotated such that x-axis direction corresponds to heading θ_0 (such as in our numerical example where $\theta_0 = \theta_{ab} = 315°$), the above formulae must be amended by replacing the argument of the trigonometric functions with $(\theta - \theta_0)$.*
- *Observe that $D\left(\mathcal{C}_L(\theta_1, \theta_2)\right) = D\left(\mathcal{C}_R(\theta_2, \theta_1)\right)$. In particular, in the case of our numerical example, $D\left(\mathcal{C}_L(\theta_{ab}, \theta_1)\right) + D\left(\mathcal{C}_R(\theta_1, \theta_2)\right) + D\left(\mathcal{C}_L(\theta_2, \theta_{ab})\right) = 2\left[D\left(\mathcal{C}_L(\theta_{ab}, \theta_1)\right) + D\left(\mathcal{C}_L(\theta_2, \theta_{ab})\right)\right]$.*

B.2 L-Synthesis Calculation

The synthesis of the numerical example in Section 4 divides the positive x-axis into three zones of optimal path types: (1) $\mathcal{CCC}$-zone, (2) $\mathcal{CSCC}$-zone and (3) $\mathcal{CSCSC}$-zone. First, we derive the L-synthesis determining the values of L that separate the different zones. Then, for a given value of L, we compute the remaining parameters of the path that completely determine an optimal path. For the $\mathcal{CCC}$ zone, the parameters of an optimal path to be determined are $\theta^1 \in [\theta_{ab}, \theta^u_{ab}]$ and $\theta^2 \in [\theta^d_{ab}, \theta_{ab}]$, which are the maximum and minimum heading angles taken by the agent along its optimal path. For the $\mathcal{CSCC}$ zone, the maximum heading angle achieves its upper bound of θ^u_{ab}, and the remaining parameters to determine are $\theta^2 \in [\theta^d_{ab}, \theta_{ab}]$, the minimum heading angle, and s_1, the length of the straight-line segment with heading θ^u_{ab}. Finally, for the $\mathcal{CSCSC}$ zone, the agent reaches both θ^u_{ab} and θ^d_{ab} along the optimal path, and the path is completely characterized by the lengths s_1 and s_2, corresponding to the two straight-line segments S_1 and S_2 that have headings θ^u_{ab} and θ^d_{ab}, respectively. Next, we write out the equations to be solved for each of the three cases that determine the parameters characterizing an optimal path from $s = a = (0, 0)$ to a given point $t = b = (L, 0)$, as well as the conditions satisfied at each partitioned zone that enable us to carry ut the computation.

B.2.1 $\mathcal{CCC}$-zone

In the $\mathcal{CCC}$-zone, an optimal path from $a = (0, 0)$ to $b = (L, 0)$ is of the form $\mathcal{C}_L(\theta_{ab}, \theta^1)\mathcal{C}_R(\theta^1, \theta^2)$ $\mathcal{C}_L(\theta^2, \theta_{ab})$, where $\theta^1 \in [\theta_{ab}, \theta^u_{ab}]$ and $\theta^2 \in [\theta^d_{ab}, \theta_{ab}]$ are the maximum and minimum heading angles traversed by the agent. In order for the path to reach point $b = (L, 0)$, the displacement of the path must be equal to $(L, 0)$, which leads to the following equation in θ^1 and θ^2:

$$D\left(\mathcal{C}_L(\theta_{ab}, \theta^1)\right) + D\left(\mathcal{C}_R(\theta^1, \theta^2)\right) + D\left(\mathcal{C}_L(\theta^2, \theta_{ab}\right) = \begin{pmatrix} L \\ 0 \end{pmatrix}.$$

Writing the equations satisfied by each coordinate of the vector and using the results from Section B.1, we obtain:

$$\int_{\theta_{ab}}^{\theta^1} R(\theta)\cos(\theta-\theta_{ab})d\theta + \int_{\theta^2}^{\theta_{ab}} R(\theta)\cos(\theta-\theta_{ab})d\theta = \frac{L}{2}, \tag{37}$$

$$\int_{\theta_{ab}}^{\theta^1} R(\theta)\sin(\theta-\theta_{ab})d\theta + \int_{\theta^2}^{\theta_{ab}} R(\theta)\sin(\theta-\theta_{ab})d\theta = 0. \tag{38}$$

Solving this system of equations for a given L yields the values of θ^1 and θ^2 that characterize an optimal path from a to b in the $\mathcal{CCC}$-zone (see Figure 51).

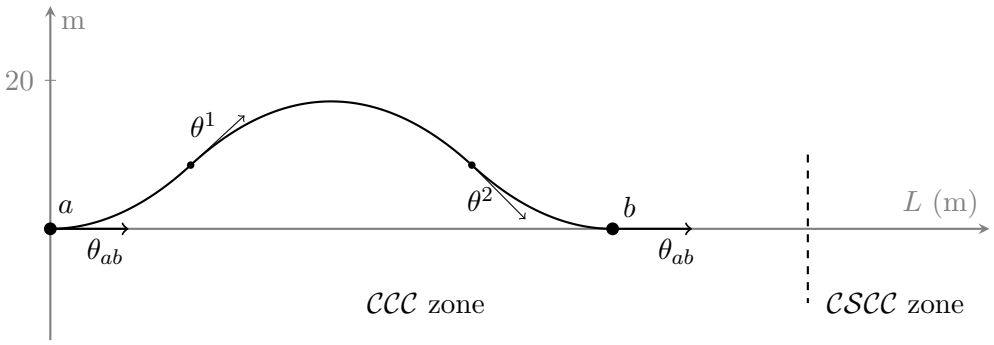

Figure 51: Example of an optimal path of form $\mathcal{CCC}$.

Given the properties of the speed function on $[\theta^d_{ab}, \theta^u_{ab}]$, θ^1 is an increasing function of L, while θ^2 is decreasing. Then, the boundary value of L for the $\mathcal{CCC}$-zone is when either one of θ^1 and θ^2 reaches its limiting bound (θ^u_{ab} for θ^1, and θ^d_{ab} for θ^2). In our numerical example, θ^1 reaches its bounding value θ^u_{ab} first, and the value of L for which this happens is the boundary of the $\mathcal{CCC}$-zone. We find it by setting $\theta^1 = \theta^u_{ab}$, solving for θ^2 in Equation (38), and then solving for L in Equation (37).

B.2.2 $\mathcal{CSCC}$-zone

In the $\mathcal{CSCC}$-zone, an optimal path from $a = (0,0)$ to $b = (L,0)$ is of the form $\mathcal{C}_L(\theta_{ab}, \theta^u_{ab})S_1$ $\mathcal{C}_R(\theta^u_{ab}, \theta^2)\mathcal{C}_L(\theta^2, \theta_{ab})$, where $\theta^2 \in [\theta^d_{ab}, \theta_{ab}]$ is the minimum heading angle reached by the agent and S_1 is a straight-line segment with heading angle θ^u_{ab} and length $s_1 = ||S_1||$. In order for the path to end at point $b = (L,0)$, the displacement of the path must be equal to $(L,0)$, which leads to the following equation in θ^2 and s_1:

$$D\left(\mathcal{C}_L(\theta_{ab}, \theta^u_{ab})\right) + D(S_1) + D\left(\mathcal{C}_R(\theta^u_{ab}, \theta^2)\right) + D\left(\mathcal{C}_L(\theta^2, \theta_{ab}\right) = \begin{pmatrix} L \\ 0 \end{pmatrix}.$$

Writing the equations satisfied by each coordinate of the vector and using the results from Section B.1, we obtain:

$$2\int_{\theta_{ab}}^{\theta^u_{ab}} R(\theta)\cos(\theta-\theta_{ab})d\theta + s_1\cos(\theta^u_{ab}-\theta_{ab}) + 2\int_{\theta^2}^{\theta_{ab}} R(\theta)\cos(\theta-\theta_{ab})d\theta = L, \tag{39}$$

$$2\int_{\theta_{ab}}^{\theta^u_{ab}} R(\theta)\sin(\theta-\theta_{ab})d\theta + s_1\sin(\theta^u_{ab}-\theta_{ab}) + 2\int_{\theta^2}^{\theta_{ab}} R(\theta)\sin(\theta-\theta_{ab})d\theta = 0. \tag{40}$$

Solving this system of equations for a given value of L yields the values of θ^2 and s_1 that characterize an optimal path from a to b in the $\mathcal{CSCC}$-zone (see Figure 52).

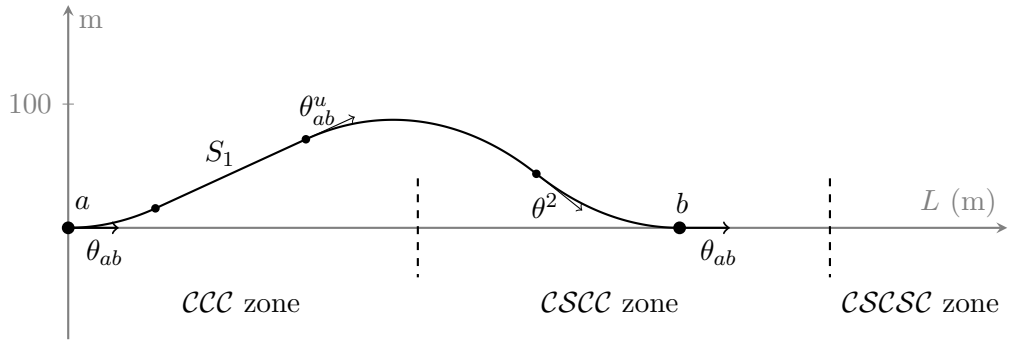

Figure 52: $\mathcal{CSCC}$ path.

θ^2 is a decreasing function of L and eventually reaches its lower bound of θ^d_{ab}, at which point the boundary between the $\mathcal{CSCC}$ and $\mathcal{CSCSC}$ zones is reached. We can find the value of L corresponding to this bound by setting $\theta^2 = \theta^d_{ab}$, solving for s_1 in Equation (40), and then solving for L in Equation (39).

B.2.3 $\mathcal{CSCSC}$-zone

In the $\mathcal{CSCSC}$-zone, an optimal path from $a = (0, 0)$ to $b = (L, 0)$ is of the form $\mathcal{C}_L(\theta_{ab}, \theta^u_{ab})S_1$ $\mathcal{C}_R(\theta^u_{ab}, \theta^2)S_2\mathcal{C}_L(\theta^2, \theta_{ab})$, where S_1 and S_2 are straight-line segments with heading angles θ^u_{ab} and θ^d_{ab} and lengths s_1 and s_2, respectively. In order for the path to end at point $b = (L, 0)$, the displacement of the path must be equal to $(L, 0)$, which leads to the following equation in s_1 and s_2:

$$D\left(\mathcal{C}_L(\theta_{ab}, \theta^u_{ab})\right) + D(S_1) + D\left(\mathcal{C}_R(\theta^u_{ab}, \theta^d_{ab})\right) + D(S_2) + D\left(\mathcal{C}_L(\theta^d_{ab}, \theta_{ab}\right) = \begin{pmatrix} L \\ 0 \end{pmatrix}.$$

The total displacement caused by the turns $\left(D\left(\mathcal{C}_L(\theta_{ab}, \theta^u_{ab})\right) + D\left(\mathcal{C}_R(\theta^u_{ab}, \theta^d_{ab})\right) + D\left(\mathcal{C}_L(\theta^d_{ab}, \theta_{ab})\right)\right.$ is fixed in the $\mathcal{CSCSC}$-zone. Consequently, let $c = (x_s, y_s) + D\left(\mathcal{C}_L(\theta_{ab}, \theta^u_{ab})\right) + D\left(\mathcal{C}_R(\theta^u_{ab}, \theta^d_{ab})\right) +$ $D\left(\mathcal{C}_L(\theta^d_{ab}, \theta_{ab}\right))$. Writing the equations satisfied by each coordinate of the displacement vector and using the results from Section B.1, we obtain:

$$s_1 \cos(\theta^u_{ab} - \theta_{ab}) + s_2 \cos(\theta^d_{ab} - \theta_{ab}) = L - x_c, \tag{41}$$

$$s_1 \sin(\theta^u_{ab} - \theta_{ab}) + s_2 \sin(\theta^d_{ab} - \theta_{ab}) = -y_c. \tag{42}$$

Then, solving this system of equations for a given value of L yields the values of s_1 and s_2 that characterize an optimal path from a to b in the $\mathcal{CSCSC}$-zone (see Figure 53).

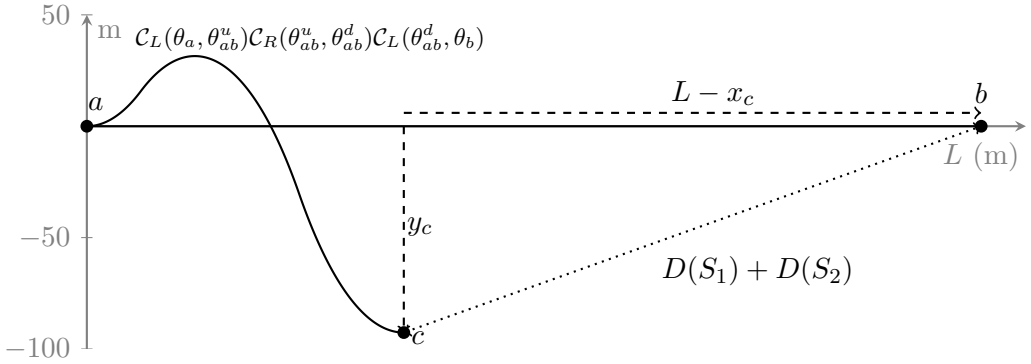

Figure 53: Decomposition of an optimal path from a to b in the $\mathcal{CSCSC}$-zone.

Funding

This work was supported in part by the Office of Naval Research through the Multidisciplinary University Research Initiative (MURI) Optimum Vessel Performance in Evolving Nonlinear Wave Fields grant (N00014-05-1-0537) and through the Autonomous Vehicle Dynamic Navigation System grant (N00014-11-1-0516).

Acknowledgment

The first author would like to thank Elmer G. Gilbert and Robert L. Smith from the University of Michigan for their helpful discussions. The authors also thank the anonymous reviewers, whose thorough and constructive feedback helped to improve this paper.

References

Bakolas, E. & Tsiotras, P. (2009). In Joint 48th IEEE Conference on Decision and Control and 28th Chinese Control Conference pp. 5649 –5654,.

Bakolas, E. & Tsiotras, P. (2010). In Proceeding of 2010 American Control Conference, Baltimore, MD.

Balkcom, D. J., Kavathekar, P. A. & Mason, M. T. (2006). International Journal of Robotics Research 25, 985–999.

Balkcom, D. J. & Mason, M. T. (2002). International Journal of Robotics Research 21, 199–217.

Bhattacharya, S., Murrieta-Cid, R. & Hutchinson, S. (2007). Robotics, IEEE Transactions on 23, 47 –59.

Boissonnat, J.-D., Cérézo, A. & Leblond, J. (1994). Journal of Intelligent and Robotic Systems 11, 5–20.

Boissonnat, J.-D., Cérézo, A. & Leblond, J. (1994). Research Report RR-2160 INRIA.

Bui, X.-N., Souères, P., Boissonnat, J.-D. & Laumond, J.-P. (1994). In Proceedings of the 11th IEEE Internatational Conference on Robotics Automation pp. 2–7,.

Chitsaz, H. & LaValle, S. M. (2007). In Proceedings of the 46th IEEE Conference on Decision and Control pp. 2379–2384,, New Orleans, LA.

Chitsaz, H., LaValle, S. M., Balkcom, D. J. & Mason, M. T. (2009). International Journal of Robotics Research 28, 66–80.

Dolinskaya, I. S., Kotinis, M., Parsons, M. G. & Smith, R. L. (2009). Journal of Ship Research 53, 121–129.

Dolinskaya, I. S. & Smith, R. L. (2012). Technical Report 12-01 Northwestern University, available at http://www.iems.northwestern.edu/research/papers.html.

Dubins, L. E. (1957). Amer. J. Math. 79, 497–516.

Filippov, A. F. (1962). Journal of the Society for Industrial and Applied Mathematics, Series A: Control 1, 76–84.

Giordano, P. R. & Vendittelli, M. (2009). Trans. Rob. 25, 1184–1191.

Giordano, P. R., Vendittelli, M., Laumond, J.-P. & Souères, P. (2006). IEEE Transactions on Robotics 22, 1040 – 1047.

McGee, T. G., Spry, S. & Hedrick, J. K. (2006). In Proceedings of the AIAA Conference on Guidance, Navigation and Control, Ketstone, Colorado.

McNeely, R. L., Iver, R. V. & Chandler, P. R. (2007). Journal of Guidance, Control, and Dynamics 30, 1299–1306.

Osborne, J. & Rysdyk, R. (2005). In Proceedings of the American Institute of Aeronautics and Astronautics Infotech@Aerospace Conference, Arlington, VA.

Pontryagin, L. S., Boltyanskii, V. G., Gamkrelidze, R. V. & Mishchenko, E. F. (1962). The mathematical theory of optimal processes. Translated from the Russian by K. N. Trirogoff; edited by L. W. Neustadt, Interscience Publishers John Wiley & Sons, Inc. New York-London.

Reeds, J. A. & Shepp, L. A. (1990). Pacific J. Math. 145, 367–393.

Rysdyk, R. (2007). Journal of Guidance, Control, and Dynamics 30, 1168–1171.

Souères, P. & Boissonnat, J. D. (1998). In Robot Motion Planning and Control, (Laumond, J.-P., ed.), pp. 93–170, Springer.

Souères, P. & Laumond, J.-P. (1996). IEEE Trans. Automat. Control 41, 672–688.

Sussmann, H. J. & Tang, G. (1991). Technical Report SYCON-91-10 Rutgers Center for Systems and Control.

Techy, L. & Woolsey, C. A. (2009). Journal of Guidance, Control, and Dynamics 32, 1736–1746.

Vendittelli, M., Laumond, J.-P. & Nissoux, C. (1999). IEEE Transactions on Robotics and Automation 15, 678 – 691.

Wang, H., Chen, Y. & Souères, P. (2009). IEEE Transactions on Robotics 25, 399–413.

Youse, B. K. (1978). Calculus with Analytical Geometry. Holt, Rinehart and Winston.